SETCOR
Conferences & Exhibitions

The Polymers 2024 International Conference

March 06 to 08 2024, Seville, Spain

Conference Proceedings

Recovering and transforming fishing waste for a sustainable future

Sónia Miranda[1], Mónica Fernandes[1], Renato Reis[1], Tânia Simões[2], João Redol[2], Pedro Manuel[3], Cristina Serralheiro[3], Pedro Ramalhete[4]

[1] Innovation in Polymer Engineering (PIEP), Guimarães, Portugal, sonia.miranda@piep.pt;
[2] Neutroplast, Sobral Monte Agraço, Portugal, taniasimoes@neutroplast.com
[3] Bitcliq, Caldas da Rainha, Portugal, pedro.manuel@bitcliq.com
[4] Justdive, Peniche, Portugal, pedroramalhete@justdive.pt

Abstract

Marine pollution, particularly arising from fishing activities, poses a significant threat to glob-al aquatic ecosystems. The improper disposal of fishing gear, such as nets and traps, contributes to the phenomenon known as 'ghost fishing,' resulting in direct harm to marine fauna and the generation of persistent waste in the aquatic environment. The unnatural presence of these substances leads to consequences such as habitat destruction, entanglement of animals, facilitation of invasive species transfers between ecosystems, and sediment deposition. These factors can have potential impacts on benthic animal life and feeding. At the forefront of environmental sustainability, the SeaRubbish2Cap project introduces an innovative approach to comprehensively tackle the issues of ocean waste recovery, with a strong emphasis on the circular economy and sustain-able recycling. To address this challenge, the project is developing a user-friendly mobile application that allows fishermen to identify and mark the locations where they lose their fishing artifacts at sea. This data aids in target-ed collection efforts and contributes to a better understanding of marine waste distribution. The located waste originating from fishing activities in the Peniche region's ocean floor was collected through a professional and careful process to minimize damage to the under-water environment. Additionally, practical strategies for proper waste treatment were thoroughly explored. This involved a multi-step process, including the meticulous removal of contaminants, segregation based on object characteristics, cleaning, and individual characterization of each waste item. Various techniques were employed to ensure thorough characterization, such as flow index (MFR), FTIR analysis (Fourier Transform Infrared Spectroscopy).

During the waste analysis, the identification of polymers and contaminants, including shell fragments from crustaceans, guided the meticulous selection of suitable elements for the treatment process. Subsequent to the comprehensive treatment procedure, a co-rotating twin-screw extruder was employed to fabricate a compound incorporating 70 wt% of recycled marine waste with polyethylene reclaimed from Neutroplast's industrial processing. The result-ant product demonstrates potential utility across various applications, effectively exemplifying the SeaRubbish2Cap project's adept response to the environmental challenge. This underscores its feasibility and success in generating valuable materials while advocating for environmental stewardship.

Keywords: Marine waste, Circular economy, Polymer compound, Waste characterization.

1. Introduction

Marine pollution poses a challenge that transcends geographical boundaries and impacts a range of vital economic sectors, including fishing, aquaculture, tourism, recreation, and maritime transport. The severity of this issue is due to the persistent degradation of plastics in the marine environment. Exposed to factors such as sunlight, mechanical stress, abrasion, oxidation, and biological biodegradation processes, these materials fragment into nano and microplastics, and became a potential threat to marine food chains and release harmful chemicals into aquatic ecosystems. Alarming estimates indicate that between 6 and 17 million tons of waste are deposited in the oceans annually, with plastics accounting for a significant proportion, ranging between 60% and 90%. The concentration of this debris is particularly high in coastal and sensitive areas due to fishing activities, heightening the urgency of effective collection and recycling measures. Initiatives such as the SeaRubbish2Cap project are emerging as innovative and integrated proposals to tackle marine pollution in a holistic way. This project not only prioritizes the efficient removal of waste from oceans, but also aims to transform it into valuable products, promoting a more sustainable and circular blue economy. Using advanced industrial processing technologies, including extrusion and blow moulding, SeaRubbish2Cap seeks to create and establish an inclusive and collaborative value chain involving a wide range of stakeholders, from divers

and fishermen to manufacturers and end consumers. This article aims to provide a detailed and comprehensive analysis of the work developed within the SeaRubbish2Cap project, exploring the key stages, challenges faced, and the potential impacts of this ground-breaking initiative (**Fig. 1**). In addition, we will examine emerging mechanical recycling technologies for marine plastics and recent advances in the incorporation of recycled materials into high value products. Through this approach, we aspire to contribute to the advancement of scientific and technological knowledge in the field of sustainable marine waste management, encouraging responsible and innovative practices in the global blue economy.
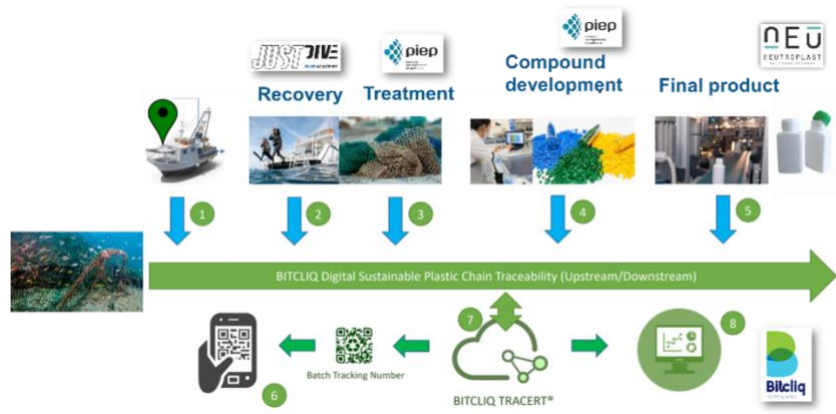
Fig. 1 - Key stages of the work developed within the SeaRubbish2Cap project.

2.   Methodology

2.1. Marine Waste Collection

Marine waste collection was conducted in targeted coastal areas known for high fishing activity. A systematic sampling approach was employed to ensure representative collection of various types of fishing waste, including nets, traps, and other discarded fishing gear. Collection sites were selected based on historical data of fishing hotspots and reports of marine litter accumulation.

A team of trained professionals operated specialized equipment for marine waste retrieval. During collection activities, care was taken to minimise disturbance to the marine ecosystem. Each collected item was carefully catalogued, photographed, and labelled with location coordinates and collection date. The collected marine waste was then transported to a designated processing facility for sorting and further characterization. Initial visual inspection and preliminary sorting were made to screen the waste into different categories based on material type and condition. This categorisation facilitated subsequent in-depth analysis and optimization of the recycling process.

2.2. Application Developed

In parallel with waste collection efforts, an innovative mobile application was developed to assist in tracking and managing marine waste data. This user-friendly application enabled real-time data entry of waste collection locations, types of waste retrieved, and quantities collected. Additionally, the application incorporated a mapping feature to visualize the distribution of marine waste hotspots and aid in strategic planning for future collection efforts.

2.3. Waste Characterization

Each fishing gear was initially shredded into small samples to facilitate handling and processing. Subsequently, 100 grams, of each fishing gear sample, were processed using a micro-extruder Xplore MC15, to ensure material uniformity. The aim of this step was to homogenise the material from each fishing gear type in order to facilitate subsequent characterisation and identification of its constituents. Fourier Transform Infrared Spectroscopy (FTIR) analysis was performed on the processed samples to identify the polymers and possible contaminants. The FTIR spectra were acquired in transmission mode using film samples prepared by hot compression from filament fragments previously obtained by extrusion, ensuring sample homogenization.

2.4. Mechanical Recycling

Mechanical recycling of the recovered fishing waste (r-Fishing) was performed using a co-rotating twin-screw extruder Coperion ZSK 26, with an L/D ratio of 40. The extrusion process involved several key steps to ensure the production of a high-quality recycled compound:

1)   Feedstock Preparation:

The r-Fising was subjected to size reduction using a granulator (RSP 2045 from Piovan), producing flakes up to 5 mm. The material was washed using fresh water at 25°C and mechanically stirred. This washing process was repeated twice to ensure the removal of contaminants and residues. The pre-treated material was finally subjected to a drying process at 60°C for 4 hours to eliminate residual moisture content.

2)   Extrusion Process:

The pre-treated r-Fishing flakes were fed into the co-rotating twin-screw extruder along with recycled polyethylene (r-HDPE) from Neutroplast's production process. The extruder was operated at a temperature profile of 220 - 230°C, a screw rotation speed of 180 rpm, a pressure of 35 – 40 bar, and a melt temperature of 235°C. The output rate was maintained at 17 kg/h.

2.5. Compound Characterization

The aim of characterising the extruded material was to determine its flow properties and suitability for further processing. The Mass Flow Rate (MFR) of the samples was determined based on the method A of ISO 1133-1 using a Göttfert MI-3 Melt Flow Indexer. The tests were carried out under the following conditions: temperature of 190°C and load of 2.16 kg. To ensure the reliability of the results, two tests were performed on each sample. The MFR of the extruded material, the r-HDPE, and the r-Fishing were measured. The analysis was to verify the suitability of the developed compound for the extrusion blow moulding process used to prototype the final product.

3.   Results and Discussion
3.1. Characterization of Fishing Waste

FTIR analyses revealed distinct features for different types of r-Fishing (**Fig. 2**). All fishing gear, except for the nets, exhibited double bands around 730 - 720 cm^{-1}, characteristic peaks of polyethylene (PE). The presence of polypropylene (PP) was identified in some r-Fishing samples, confirmed by the bands at 1376 and 1166 cm^{-1}. In contrast, the nets displayed a band pattern indicative of the presence of polyamide 6 (PA6), centred around 3300, 3080, 1640, 1540, 1263, 1204, 1171, 693, and 580 cm^{-1}.

Given Neutroplast's use of PP and PE in its manufacturing operations, these materials were selected as the primary focus for recycling and compound development. The PA 6 found the r-Fishing has been allocated to alternative research as it is not part of Neutroplast's existing material portfolio.

3.2. Compound Development

After the treatments, the co-rotating twin-screw extruder Coperion ZSK 26, was used for compound formulation. With the 35 kg of r-Fishing previously recovered, a composition was established in which approximately 30 wt% of these materials were incorporated into r-HDPE. A total of 100 kg of pellets of fishing waste recycled (FWR) were produced. The r-HDPE was recovered from Neutroplast's production process, resulting in a compound developed from 100% recycled material.

3.3. Compound Characterization

The MFR of the FWR, the r-HDPE from Neutroplast's process, and the r-Fishing were measured (**Table 1**). The FWR showed an MFR value very close to that of r-HDPE. This consistency shows that the FWR has similar flow characteristics, making it compatible with Neutroplast's existing processing equipment and processes. The flow properties required for processing were not compromised by the incorporation of 30 wt% r-Fishing into the r-HDPE matrix.
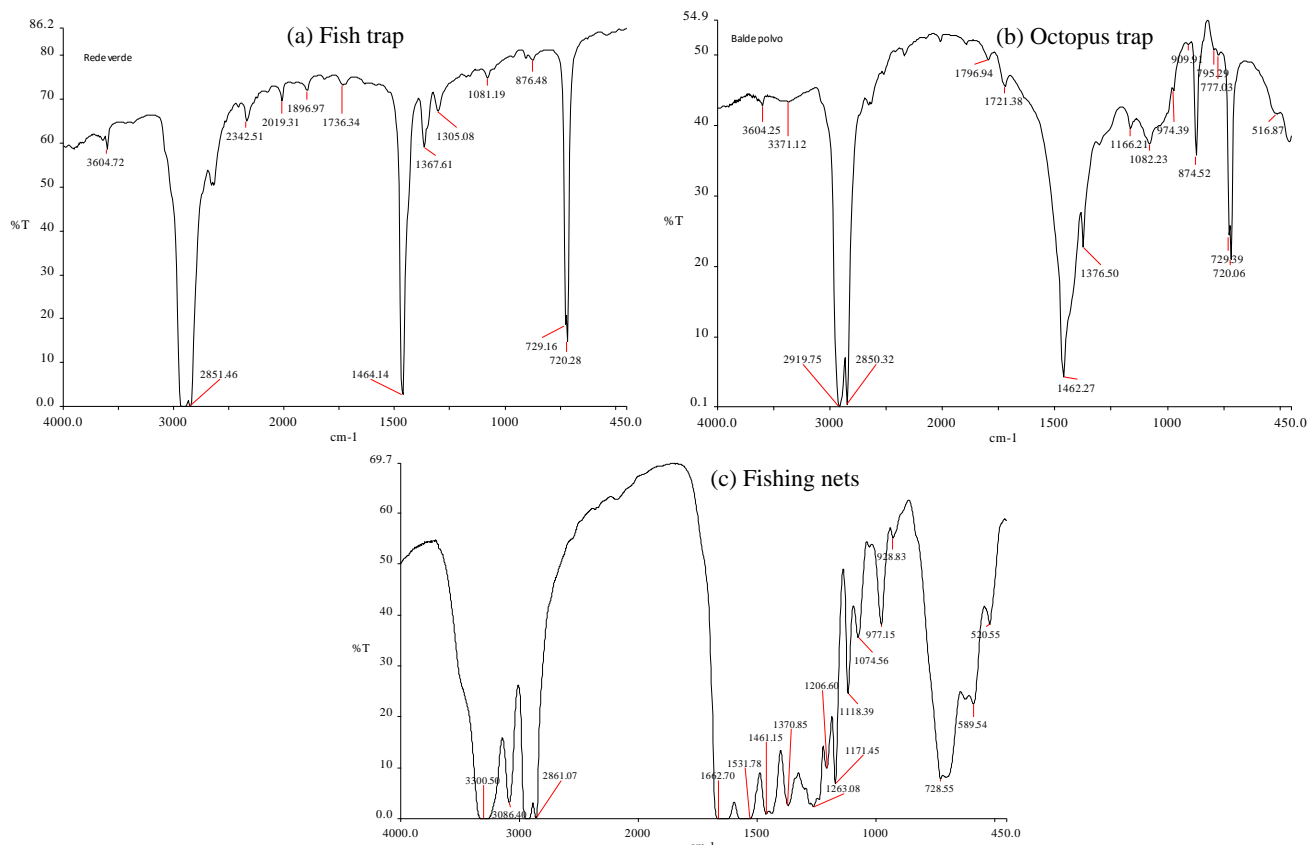
Fig. 2: FTIR spectrum obtained from the analysis of the materials recovered from the deep sea.

Table 1: MFR values obtained from the analysis of the materials used on the extrusion process and the final product.

Material	r-HDPE	r-Fishing	FWR (r-HDPE + 30 wt% r-Fishing)
MFR (g/10 min)	0,59 ± 0,00	0,47 ± 0,00	0,52 ± 0,00

4. Conclusion

The SeaRubbish2Cap project demonstrates the feasibility of transforming marine waste, specifically fishing waste, into high-value products through mechanical recycling. During our characterization process, we found that a large part (73%) of fishing waste is composed of PE. Cage traps were the most commonly found waste, yet they also pose significant challenges for recovery due to their structure and composition. Nevertheless, the FWR compound produced in this project showed a similar MFR when compared to the r-HDPE from Neutroplast's process, indicating its suitability for the extrusion blow moulding process.

Despite the potential for recycling marine waste, our experience suggest that recycling facilities are not yet fully equipped or ready to handle this specialized waste stream. The recycling of marine waste is also hindered by its high cost attributed to manual labour required for the recovery from the deep sea and sorting of materials.

This innovative approach contributes to environmental protection, promotes sustainable practices in the global blue economy, and emphasizes the importance of waste recovery and recycling. Moving forward, it is essential to address the challenges associated with marine waste recycling, by improving the recycling facilities' and developing cost-effective solutions to make the recycling process more accessible and economically viable. Collaborative efforts involving policy makers, industry stakeholders, and environmental organisations are crucial finding sustainable waste management practices and reducing the environmental impact of marine pollution.

Analyzing the Influence of Color Masterbatch on the Injection Molding of Post-Industrial Plastic Waste

Magdalena Pöttinger[1,*], Christian Marschik[1], Klaus Straka[2], Klaus Fellner[3], Georg Steinbichler[2]

[1] Competence Center CHASE GmbH, Hafenstraße 47-51, 4020 Linz, Austria
[2] Institute of Polymer Injection Moulding and Process Automation, JKU - Johannes Kepler University Linz, Altenberger Straße 69, 4040 Linz, Austria
[3] ENGEL AUSTRIA GmbH, Ludwig-Engel-Straße 1, 4311 Schwertberg, Austria

Abstract

In injection molding, achieving a uniform color is essential to product quality. Achieving this is challenging when using virgin polymers, but becomes even more difficult when processing recycled plastic waste, which typically contains contaminants that can affect the optical properties of an injection-molded part. One approach to keeping product color constant despite inhomogeneous input materials is to add color masterbatch. For quality assurance purposes, we experimentally investigated the minimum amount of masterbatch to be added to achieve a defined color of an injection-molded part made from recycled material. To this end, we fabricated discs using mixtures of color masterbatch with virgin and recycled (shredded post-industrial waste) materials. Using a single-stage injection molding process, plastic flakes were directly processed without the intermediate step of regranulation. The process involved a robotic arm removing the part from the mold and transferring it to a photobox that guaranteed constant lighting conditions during measurement with integrated inline color and temperature sensors. The masterbatch concentration in the input material was systematically varied to determine the minimum content required for achieving a defined reference color derived from discs made from virgin material and the recommended 2 wt% of masterbatch. Our experiments demonstrate the potential for more economical use of masterbatch when processing recycled material. The color sensor further allowed us to adjust the masterbatch content during the process, as the color of each injection-molded part was measured inline in real time. This provides the basis for an automated control of masterbatch dosing.

Keywords: injection molding, plastic recycling, inline measurement, process analysis, automation, optical properties, color.

1. Introduction

Visual appearance plays a critical role in the quality assurance of injection-molded parts [1-2]. Coloring virgin material with masterbatch (MB) results in almost perfectly consistent color of the components produced. Adding recycled material to the mixture, however, typically alters the color obtained [3]. Since the EU has set ambitious targets for plastic recycling, thus requiring increased recycling rates, color and processing behavior of recycled materials must be investigated as part of quality insurance [4, 5]. The color of the recycled material may affect the color of the injection-molded part either positively or negatively, depending on whether it is similar to that of the MB used and thus to the color to be achieved. If recycled material and MB are dissimilar, achieving a predefined reference color becomes more challenging and requires a higher amount of MB content. There are two main types of plastic waste: post-consumer and post-industrial waste [6]. In this paper, we demonstrate how MB can be used more economically when using post-industrial plastic waste that has been suitably sorted according to color and material characteristics.

2. Experimental

In the experiments, an ENGEL e-mac 180 injection molding machine, as shown schematically in Figure 1, was used. For each mix of material, the color of the injection-molded part was measured because it is homogeneous, allowing the color values for each component to be stored individually [7]. Color measurements were performed using a True Color Sensor (TCS) and an IR-pyrometer integrated into a photobox. The photobox was used to minimize the influence of ambient light. The TCS was designed to resemble the human eye and provide information about the color of the component [8, 9]. The

pyrometer was installed to measure the color after demolding of the part. Temperature was measured at this position because color is temperature-dependent, a phenomenon also known as thermochromism [10]. Distance spacers were attached to the photobox to ensure a uniform measurement distance. A robotic arm removed each component from the mold and held it in front of the sensors for 5 seconds, during which time the measurement was conducted. The part was subsequently transported to a conveyor belt below the photobox and placed on it. The test components were circular discs with a diameter of 150 mm and a thickness of 2 mm. To simulate post-industrial waste, components were first injection-molded using a mixture of virgin polypropylene (PP) material and 2 weight percent (wt%) of green MB, and then shredded into recyclate flakes.
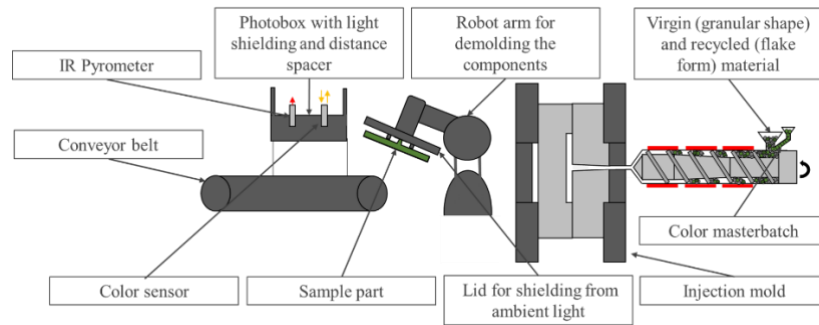
Fig. 1: Setup for inline color measurement in the injection molding process.

The color values of the injection-molded discs measured were represented in the $CIE\ L^*a^*b^*$ color space, which is widely used in industry [11]. Evaluating the difference (ΔE) between two colors in this space requires knowledge of the L^*, a^* and b^* values, where L^* defines brightness, while a^* and b^* describe red-green and yellow-blue chromaticity and color intensity, respectively. The ΔE^*_{ab} value can be calculated as follows [12]:

$$\Delta E^*_{ab} = [(\Delta a^*)^2 + (\Delta b^*)^2 + (k\Delta L^*)^2]^{1/2}, \qquad (1)$$

where $k = 1$ for samples close in color space. The following classification can be used to categorize the ΔE values: If ΔE lies between 0 and 1, no differences can be perceived by the human eye. Only a trained eye may detect differences for ΔE values between 1 and 2, and color differences become generally noticeable for ΔE values of 2 and above [13].

The proportions of virgin and recycled material used in the experiments are shown in Table 1. First, discs were produced using a mixture of virgin polypropylene (PP) material and 2 wt% green MB. This MB content is typically recommended by MB manufacturers, depending on the thickness and surface of the component. Using the experimental setup shown in Figure 1, the color values of 10 injection-molded parts produced with this mixture were measured after demolding, and their mean was set as the reference color. Subsequently, the recyclate-based components were measured, for which material mixtures comprising virgin material, recycled flakes, and green MB were prepared as listed in Table 1. The color of the recyclate closely resembled the color hue of the MB. The recycled flakes were processed directly on the injection molding machine without regranulation. For each material mixture (virgin, recycled and MB material), 30 components were produced. The color values of 10 parts that were injection-molded after the process had stabilized were taken, and the mean value was calculated. The objective was to approach the reference color by adding green MB in Experiments 2-4 while keeping the MB content minimal. Each experiment started with a MB content of 0 wt%, which was then increased step-wise by 0.5 wt%. At the point in time when the ΔE was below 2, this was seen as the optimum MB setting. For Experiment 1, however, all MB steps were tested up to a maximum of 4 wt% MB.

Table 1: Material mixtures for the color measurements.

Ex. #	Virgin material (PP) [wt%]	Recyclate (PP) [wt%]	MB content [wt%]	Recyclate Color	MB Color
1	100	-	2		Green
2	90	10	0-4	Green	Green
3	80	20	0-1	Green	Green
4	70	30	0-0.5	Green	Green

3. Results and Discussion

The measurement of the reference color yielded mean values of $L^* = 81$; $a^* = -30$ and $b^* = 50$ with standard deviations of $SD_{L^*} = 1.2$, $SD_{a^*} = 0.5$ and $SD_{b^*} = 1.0$. These values were set as the reference color and are indicated by the dotted lines in Figure 2, which presents the color values measured in Experiment 2. On the left y-axis the $L^*a^*b^*$ color values are plotted, and on the right y-axis the ΔE values between reference color and actual color value are plotted. On the x-axis, the MB weight fraction is indicated. Note that all MB proportions (from 0 to 4 wt%) are shown to demonstrate that no color changes were observed (i.e., $\Delta E \leq 2$) when more than 0.5 wt% MB was added, from which we conclude that adding further MB was wasteful because the color had already reached its saturation point. For the input material mixture in Experiment 2 and no MB added (i.e., 0 wt%), a ΔE of 17.82 indicated that the color achieved was not sufficiently similar to the reference color.
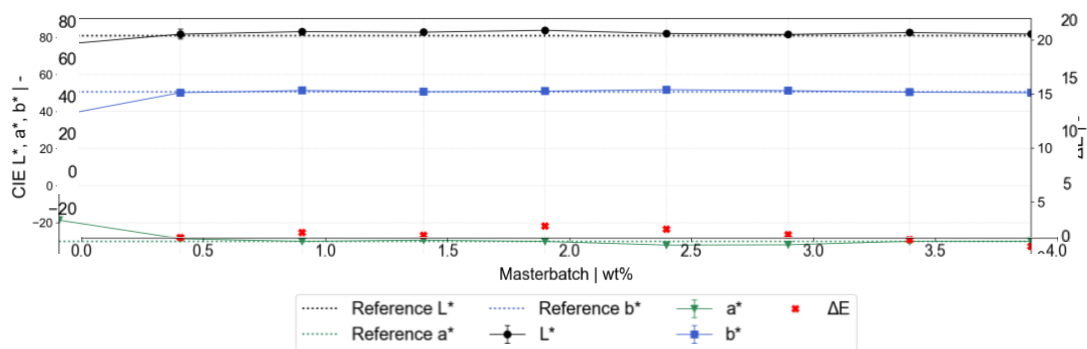
Fig. 2: Color values from Experiment 2.

For the input materials with higher recyclate content in Experiments 3 and 4, however, the ΔE values for 0 wt% MB added were 9 and 2.2, and thus lower (see Figure 3). This was due to the recyclate having a similar hue as the reference color. Additionally, the results indicate that a MB content of 0.5 wt% was sufficient to achieve a ΔE less than 2 and that addition of more MB was, again, wasteful.

(a)   (b)
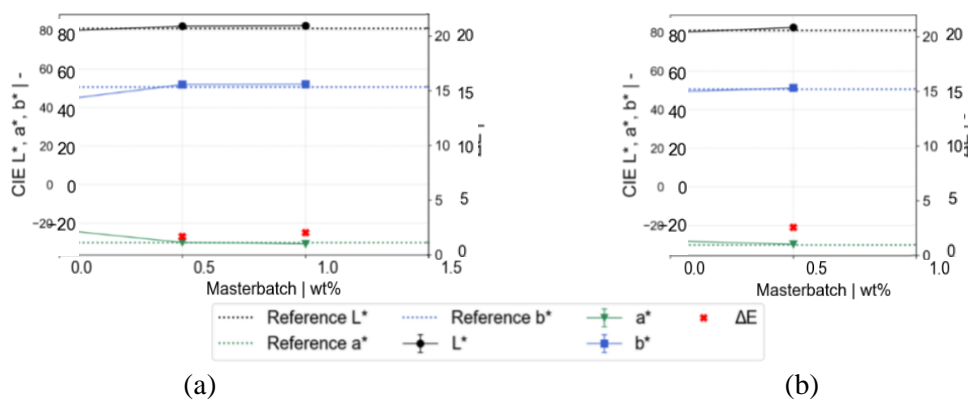
Fig. 3: Color values from Experiments 3 (a) and 4 (b).

We observed that adding recycled material allowed us to reduce the amount of MB used because they were very similar in color: MB contained in the recyclate also contributed color to the part. In Table 2,

the percentages present in the recyclates for the mixtures are provided, which can only be obtained with accurate information about the recyclate. Additionally, the sufficient MB addition in the processing is given, as determined during the measurements. The MB saving potential resulting from the use of recyclate is also shown. This has been calculated based on the MB content recommended by the MB manufacturer (2 wt%), subtracting the amount required to achieve a ΔE less than 2. Finally, the sum of MB present in the final part, including recycled and added MB, is provided. The most important insight from this Table 2 is the MB saved by processing recyclate and virgin material, which in this case was 1.5 wt%.

Table 2: Masterbatch saving potential.

Ex. #	MB in recyclate [wt%]	MB addition sufficient for the mixture [wt%]	MB saving [wt%]	Sum of MB in final part [wt%]
2	0.2	0.5	1.5	0.7
3	0.4	0.5	1.5	0.9
4	0.6	0.5	1.5	1.1

4. Conclusion

In this study, we have demonstrated that by adding post-industrial plastic waste to virgin material, masterbatch can be saved if the masterbatch and the recycled material have similar color hues. We have shown that for material mixtures containing 10 wt%, 20 wt%, and 30 wt% recylate, a masterbatch content of 0.5 wt% was sufficient to achieve a ΔE less than 2 and thus a close match to the reference color. Due to saturation effects, increasing the amount of recyclate did not significantly impact the color. Since our results show that the reference color could be achieved by adding a minimal amount of masterbatch to the recyclate, it is logical to question whether waste of masterbatch can also be prevented in the initial production process. For material mixtures with 10 wt%, 20 wt%, and 30 wt% recyclate, 1.5 wt% of masterbatch was saved in each case. In the future, masterbatch contained in recyclate could thus be employed particularly in industrial scenarios, where waste sorted according to color and material is readily available.

Acknowledgements

References

1. E. Baur, S. Brinkmann, T.A. Osswald and E. Schmachtenberg, *Saechtling Kunststoff Taschenbuch.* München, Carl Hanser Verlag, 2013.
2. R. Abrams, M. Ali, P. Denton, J. Igualada et al., "Colouring plastics: fundamentals and trends," in *Plastics, Additives and Compounding*, 2001, pp. 18-25.
3. F. Chacon, M.T. Brouwer and E.U.T.v. Velzen, "Effect of recycled content and rPET quality on the properties of PET bottles, part I: Optical and mechanical properties," in *Packaging Technolgoy and Science*, 2019, pp. 347-257.
4. A. Tenhunen-Lunkka, T. Rommes, I. Vanderreydt and L. Mortensen, "Greenhouse Gas Emission Reduction Potential of European Union's Circularity Related Targets for Plastics," in *Circular, Economy and Sustainability*, 2023, pp. 475-510.
5. European Parliamentary Research Service, "Revision of the Packaging and Packaging Waste Directive," 2023
6. S. Huysman, J. Schaepmeester, K. Regaert, J. Dewulf and S. Meester, "Performance indicators for a circular economy: A case study on post-industrial plastic waste," in *Resources, Conservation and Recycling*, 2017, pp. 46-54.
7. J. Botos, N. Murail and P. Heidemeyer, "Color measurement of plastics - From compounding via pelletizing, up to injection molding and extrusion", 29th International Conference of the Polymer Processing Society - Conference Papers, 2014, pp. 16-19.

8. K. Jensen and T. Nimz, ”Welche Genauigkeiten erreicht man mit Farbsensoren und Mini-Spektrometern?”, in *MAZeT Electronic Engineering and Manufacturing Services*, 2013.

9. F. Nitsche, ”Optoelektronische Sensoren Für eine farbstabile LED-Ansteuerung im Passagierflugzeug”, in *Elektroniknet*, 2016.

10. J. Hiltunen, P. Silfsten, T. Jaaskelainen and P.S. Parkkinen, "A qualitative description of thermochromism in color measurements," in *Color Res.* Appl. 27, 2002, pp. 271 – 275.

11. Y. Ohno, "CIE Fundamentals for Color Measurements," in *International Conference on Digital Printing Technologies*, 2000, pp. 540-545.

12. R. W. G. Hunt, *The reproduction of colour.* 6th ed., John Wiley and Sons, Hoboken, 2006, pp. 92-125.

13. W. S. Mokrzycki, M. Tatol, "Colour difference ΔE - A survey," in *Machine Graphics and Vision*, 2011.

Surface and mechanical properties of polymer nanocomposite PVDF-HFP/PVP/SiO$_2$ with anti-fouling properties

Urška Gradišar Centa [1*], Meta Sterniša [2], Lidija Slemenik Perše [1]

[1] Laboratory for Experimental Mechanics, Faculty of Mechanical Engineering, University of Ljubljana, Aškerčeva Ulica 6, 1000 Ljubljana, Slovenia, urska.gradisarcenta@fs.uni-lj.si, lidija.slemenik.perse@fs.uni-lj.si

[2] Department of Food Science and Technology, Biotechnical Faculty, University of Ljubljana, Jamnikarjeva 101, 1000 Ljubljana, Slovenia, meta.sternisa@bf.uni-lj.si

Abstract

In this paper, a polymer nanocomposite based on PVDF-HFP and PVP polymers with mesoporous silica nanoparticles was presented as a potential material for use in contact surface applications. The surface morphology and the degree of agglomeration of nanoparticles in these coatings also depend on the amount of PVP polymer. The higher the PVP polymer content, the smoother the surface of the coatings. Higher proportion of SiO$_2$ nanoparticles leads to higher stiffness of the surface, which represents unfavourable surface properties for the adhesion of bacteria. The highest stiffness and Young's modulus were determined for the sample with 20 wt.% of SiO$_2$ and 20 wt.% of PVP polymer. The highest elasticity of the coatings with SiO$_2$ content of 10 wt.% was determined for the coatings with the highest PVP polymer content (40 wt.%). The mesoporous SiO$_2$ nanoparticles act as a structural and functional materials in this polymer matrix, which also has an effect on the stiffness and anti-fouling activity. A statistically significant anti-fouling activity at 37 °C was observed for Gram-negative bacterium *Escherichia coli* after 4 and 24 hours, while a lower reduction was observed for Gram-positive bacterium *Staphylococcus aureus*. The antimicrobial activity of these coatings was not observed for either bacteria.

Keywords: Polymer nanocomposite, silicon dioxide nanoparticles, mechanical properties, surface properties, anti-fouling properties

1. Introduction

Silica (SiO$_2$) is one of the most common components of the earth's crust and the main constituent of sand. It can be extracted naturally from food waste or plants. Crystalline and amorphous silica occur in nature, and various silica derivatives can be obtained by chemical methods [1]. Nanoparticles of silicon dioxide (SiO$_2$) are used as structural materials in various fields such as microelectronics, the food and pharmaceutical industries, biomedicine, catalytic technology and sensing [2]. In recent years, silica-based antimicrobial materials have gained much attention due to the problem of microbial colonization. In these materials, the addition of silica improved the mechanical properties and increased the activity of the antimicrobial compound used (e.g. ciprofloxacin, chitosan) [1]. However, the use of antimicrobial compounds can promote the development of resistant microbial strains [3], which represent a major global health problem with an increasing number of deaths and economic burden s every year [4]. Therefore, the development of materials that prevent bacterial colonization but do not cause resistance is necessary.

The problem of microbial contamination of surfaces arises in various public and industrial surfaces. Therefore, more and more surface coatings are being developed based on polymers with antifouling and antimicrobial properties. The contact surfaces in various environments come in contact with bacterium and other microorganisms.

Microbial adherence is the first step in the process of surface colonization and subsequent biofilm formation and maturation. Biofilms are structured microbial communities that play an important role in the persistence of biofoulings in medical and industrial environments by providing mechanical stability and protection from adverse environmental conditions [5]. Bacterial adhesion is possible on any abiotic surface and involves physicochemical and molecular interactions. It is influenced by bacterial and environmental factors (temperature, pH value, humidity, contact time, bacterial strain, bacterial concentration) but can also be modulated by the properties of the material surface – surface charge density, wettability, roughness, stiffness and surface topography [5]. These properties can be exploited for the development of new anti-fouling materials

that follow the strategy of biofilm control by preventing bacterial adhesion in its initial stage. Once the biofilm is formed, it becomes extremely difficult to mechanically remove or kill bacteria in biofilms on the solid surfaces.

Numerous polymers and their blends offer a wide range of possibilities for the development of the materials with the above- mentioned properties [6]. In previous work, we have successfully used PVDF-HFP/PVP blend as a carrier for antimicrobial MoO_3 nanowires that prevented biofilm formation on functionalized surfaces [7]. PVDF-HFP/PVP blend has already been proved to improve surface properties [8]. In the present work, we have investigated the addition of silica nanofiller.

In the present work, we have studied the addition of silica nanofiller in polymer nanocomposites, based on the combination of the polymers PVDF-HFP (poly(vinylidene fluoride-co-hexafluoropropylene)) and PVP (polyvinylpyrrolidone), prepared by the solution casting method with different mass ratio of the components. The aim of our study was to optimise the mass ratio of the components used based on the surface and mechanical properties and to test the selected blend ratio for its antimicrobial and anti-fouling activity against *Staphylococcus aureus* and *Escherichia coli*.

2.   Materials

Polymer nanocomposites were prepared using a solvent casting method. The dimethyl-formamide (DMF) was used as a solvent for poly(vinylidene fluoride-co-hexafluoropropylene)-PVDF-HFP and polyvinylpyrrolidone-PVP polymer. Both polymers were dissolved in separate vials on the magnetic stirrer (300 rpm) at 80°C for 2h. SiO_2 nanoparticles were added to the PVP polymer solution and mixed again at the same conditions. The PVDF-HFP solution and the PVP polymer dispersion were then mixed for another 2 hours (300 rpm, 80 °C) to allow the polymerization. The resulting polymer-nanocomposite dispersion was casted on a Teflon plate and the solvent started to evaporate (2 hours, 80 °C). After the preparation process, the samples were stored in a closed vacuum bag. The samples contained different amounts of PVP and PVDF polymer at the same concentration of nanofiller, in one case the sample contained twice the amount of nanofiller. The sample labelled PN1 consisted of 70 wt.% PVDF-HFP and 20 wt.% PVP polymer, sample PN2 consisted of 60 wt.% PVDF-HFP and 30 wt.% PVP and sample PN3 consisted of 50 wt.% PVDF-HFP and 40 wt.% PVP. For all three samples, the proportion of the nanofiller SiO_2 was set at 10% by weight. Sample PN4 contained 60 wt.% PVDF-HFP, 20 wt.% PVP and 20 wt.% SiO_2. To determine the antimicrobial and anti-fouling activity, the reference sample (PN5) was prepared without nanofiller SiO_2 with a composition of 75 wt.% PVDF-HFP and 25 wt.% PVP.

3.   Methods

The topography of the samples was investigated with optical microscope Keyence VHX 7000 (Keyence international, Belgium). The mechanical properties of the polymer nanocomposites were evaluated with uniaxial tensile tests on modular compact rheometer MCR 702 (Anton Paar, Austria) at room temperature. The dimensions of the samples were 5 mm in width and 40 mm in length. The thickness of the samples was around 150 µm. The sample was prefixed with the force 0.3 N. All measurements were performed on 3 samples. The average force-displacement curves are presented in Figure 1.

The antimicrobial and anti-fouling activities were tested on two bacterial strains – Gram-positive *Staphylococcus aureus* ATCC 25923 and Gram-negative *Escherichia coli* ATCC 11229 – according to the method described in Sterniša et al. [9]. The samples were incubated at a temperature of 37 °C for 4 and 24 hours.

4.   Results and Discussion

The force-displacement curves are shown in Figure 1A. The highest stiffness of the nanocomposites was observed for the sample PN4 with twice the amount of SiO_2 nanoparticles. This means that the addition of SiO_2 nanoparticles into the nanocomposite, which act as nucleators, increases the network formation of polymer chains around the nanoparticles. Consequently, a higher rigidity of the molecular structure of the nanocomposite was observed.
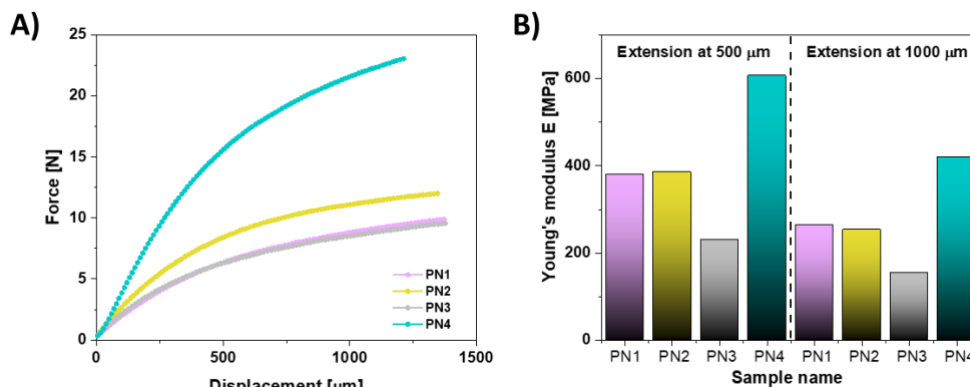
Figure 1. Mechanical properties of the polymer nanocomposite samples obtained with uniaxial mechanical tests. (A) Force-displacement curves, (B) values of Young's modulus.

The highest elasticity (Figure 1B) of the nanocomposite was observed in sample PN3 with a slightly higher concentration of PVDF-HDFP polymer (50 wt. % PVDF-HFP and 40 wt.% PVP polymer). The highest elasticity results from the fact that the PVP has shorter polymer chain compared to the PVDF-HFP polymer and therefore the PVP chains have a higher mobility. No SiO_2 agglomerations or other inhomogeneities were observed in this sample indicating good dispersion of the particles.
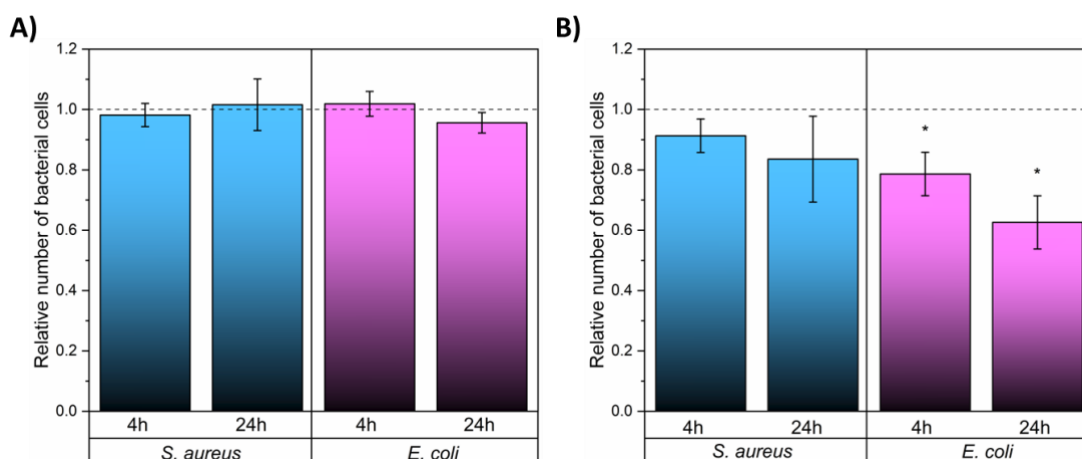
Figure 2. Antimicrobial (A) and anti-fouling (B) activity of sample PN1 regarding to PN5 on *Staphylococcus aureus* and *Escherichia coli* at the temperature of 37 °C. Asterisk (*) indicates significant difference ($P<0.05$) from control sample PN5.

The antimicrobial (Figure 2A) and anti-fouling (Figure 2B) activity was evaluated by the number of planktonic and adhered cells on the polymer nanocomposite surface. The number of planktonic cells of both bacteria did not change significantly during the 24-hour incubation, therefore the antimicrobial activity of the surface coatings was not observed. The relative number of adhered cells of the bacterium *S. aureus* was reduced by 0.01 and 0.16 after 4 and 24 hours, respectively. The strongest anti-fouling activity was observed with the bacterium *E. coli*, where the relative number of adhered cells was reduced by 0.21 and 0.37 after 4 and 24 hours of incubation, respectively.

5.   Conclusion

The results showed that the surface morphology and smoothness of the coatings were controlled by the amount of PVP polymer in the nanocomposite. A higher proportion of mesoporous SiO_2 nanoparticles with high specific surface area in the nanocomposite increased the stiffness, which is an important factor in the development of anti-fouling materials. On the other hand, the highest proportion of PVP polymers in the nanocomposite increased the elasticity of the nanocomposite due to its amorphous nature and shorter polymer chains, which enable disentanglement and thus higher flexibility. Significant anti-fouling activity against Gram-negative *E. coli* was observed, which could mean that anti-fouling activity of the prepared material is dependent on the bacterial cell wall structure.

Acknowledgements

References

1. B. Tian et al., Antibacterial applications and safety issues of silica-based materials: A review, Int J Appl Ceram Technol. 18, 289-301, 2021.
2. A. A. Nayl et al., Recent progress in the applications of silica-based nanoparticles, RSC Advances, 12, 13706–13726, 2022.
3. L. Dieltjens et al., Inhibiting bacterial cooperation is an evolutionarily robust anti-biofilm strategy, Nat Commun 11, 107, 2020.
4. A. N. Poudel et al., The economic burden of antibiotic resistance: A systematic review and meta-analysis, PloS one, 18(5), e0285170, 2023.
5. S. Zheng et al., Implication of Surface Properties, Bacterial Motility, and Hydrodynamic Conditions on Bacterial Surface Sensing and Their Initial Adhesion. Front. Bioeng. Biotechnol. 9, 643722, 2021.
6. I. Babutan et al., Antimicrobial Polymeric Structures Assembled on Surfaces, Polymers, 13(10), 1552, 2021.
7. U. Gradišar Centa, et al., Novel nanostructured and antimicrobial PVDF-HFP/PVP/MoO_3 composite, Surface Innovations, 9(5), 256–266, 2020.
8. U. Gradišar Centa et al., The effect of PVP on thermal, mechanical, and dielectric properties in PVDF-HFP/PVP thin film, Coatings, 12, 1241, 2022.
9. M. Sterniša et al., Pseudomonas fragi biofilm on stainless steel (at low temperatures) affects the survival of *Campylobacter jejuni* and *Listeria monocytogenes* and their control by a polymer molybdenum oxide nanocomposite coating, Int J Food Microbiol, 394, 110159, 2023.

Effect of a nanocellulose on the optical and mechanical properties of flax pulp

Josef Bárta[1], Kateřina Hájková[1], Adam Sikora[1]

[1] Faculty of Forestry and Wood Sciences, Czech University of Life Sciences Prague,
Kamýcká 129, 165 00 Prague, Czechia

Abstract

In the interest of our times, novel or modified materials are studied to create and enhance today's materials. Flax pulp is used because of its higher mechanical properties. This paper modified this material with the addition of nanocellulose to determine/assess the possibility of increasing some of the properties. Mechanical examinations assessed differences in properties, such as tensile strength, breaking length, and tensile energy absorption. For further determination, an optical examination was performed to evaluate colour differences in individual materials produced in this work. Different types of applications were compared to paper without the addition of nanocellulose. Specifically, nanocellulose was added to pulp mass and applied to a paper by spraying, coating, and lastly by using ultrasound. Results for mechanical properties are best for application form of spraying in terms of least use nanocellulose (3.5%) and the highest mechanical properties in most cases compared to reference paper product. The colour difference is the highest for those applications, where nanocellulose addition was more sufficient for two-layer coating, spraying, and using ultrasound. Data from this work serve as an extension to nanocellulose utilization for paper products, whether it may enhance specific properties of modified material.

Keywords: modified paper, nanocellulose, soda flax pulp, tensile strength, colour difference

1. Introduction

Starting with the selection of flax pulp, flax pulp is usually used as a high-quality pulp for special purposes due to its high strength. It is assumed, that those properties may be enhanced further with the modification of nanocellulose. Therefore, this paper evaluates certain mechanical properties with optical properties of researched pulp.

Nanocellulose is a promising material that requires further investigation for its wide range of applications. In this paper, several types of applications were chosen to determine suitability for flax pulp. Firstly, nanocellulose was added into the pulp with different ratio and then another type of applications was final coating of paper products such as spraying, coatings and ultrasounds nanocellulose applications.

Some studies have already assessed the effect of nanocellulose [1-8] with a different approach of applications. Another studies [9-11] confirmed, that some properties can be enhanced with the application of nanocellulose.

2. Materials and methods

2.1. Materials

Firstly, for the pre-experiments, kraft pulp from conifers was used given from Mondi Štětí (Štětí, Czechia). Unbleached kraft pulp had two different Kappa numbers of 24.9 and 49.7 and bleached kraft pulp was with Kappa number of 19.2 Soda flax pulp from the Delfort Group (Olšany, Czechia) with Kappa number of 19.9 was used for the following research.

2 types of nanocellulose were used, CNF-Slurry-SMC nanofibrils and TEMPO-oxidized nanofibrils from CelluloseLab (Fredericton, Canada). Both were manufactured from softwood kraft pulp, hardwood kraft pulp, kenaf pulp, and cotton pulp.

2.2. Application of nanocellulose fibrils

Two kinds of applications were chosen, incorporating nanocellulose fibrils into the pulp with 0.5,1.0, 3.0 and 5.0% of the CNF-Slurry-SMC and the second application as a surface treatment with TEMPO-oxidized nanofibrils different amount of nanocellulose fibrils through spraying, coatings and ultrasounds application.

Table 1: Characteristics of cellulose nanofibrils.

Nanocellulose type	Width	Length	Form
CNF-Slurry-SMC	30–80 nm	Up to several hundred μm	1–20% solids in the solution
TEMPO-Oxidized	20–50 nm	0.5–80 μm	0.5–3% solids in the solution

2.3. Mechanical properties

Samples were firstly conditioned before measuring mechanical properties according to TAPPI T 402 sp-008 [12]. The following tensile properties were measured according to ČSN EN ISO 1924-2 [13] on measuring equipment FRANK-PTI (Birkenau, Germany). Other mechanical properties measured were breaking length and tensile energy absorption. Optical properties were measured according to ČSN EN ISO/CIE 11664-4 [14] with equipment Konica Minolta CM-600d (New Jersey, USA). All mechanical properties were measured on at least ten samples, optical properties were measured at least five times per one sample, all results were statistically processed. For the scanning electron microscopy (SEM), samples were mounted on specimen stubs, sputter-coated with gold in the Sputter Coater JFC-1300 (Tokyo, Japan) under argon atmosphere. Then examined by scanning electron microscopy with JEOL JSM-IT500HT equipment (Tokyo, Japan) under 15 kV.

3. Results

Parameter L changes not significantly for the application of NC into the mass until 5.0% of NC applications with an increasing number in parameter L more into the white colour in comparison to reference, with the application of NC as coating and spraying has also not changed significantly, but with. higher variability for 2 coatings, spraying and ultrasound in comparison to the reference.

Incorporating nanocellulose into the pulp does not change parameters a significantly, but starting with nanocellulose application as a surface treatment, 2-layer coating changed parameter more than previous application types but with higher variability, the more obvious changes for parameter a are for spraying and ultrasound application of nanocellulose.

There is not a significant difference in b* parameter changes for the application of NC into the mass. The 1-layer coating has a significant change in parameter with lower variability than other applications like 2 coatings, spraying and ultrasound. Applications of NC as coating, spraying and ultrasound change parameter b* more into the yellow colour spectre. All details are in the following Figure 1.

(a) (b)
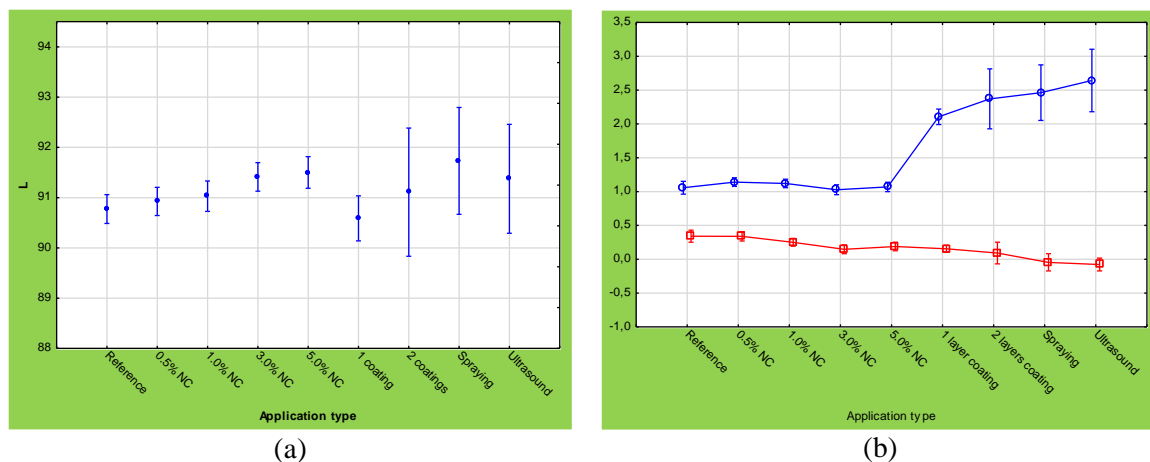
Fig. 1: (a) Parameter L, (b) parameter a* and parameter b* changes.

The dependence between tensile work absorption on the tensile index with the correlation of selected characteristics with 95% confidence interval in Figure 2 (a). with r=0.90874, there is a strong positive correlation, so when the tensile work absorption index increases, the tensile index will also increase with very strong dependence.

Tensile index results are in Figure 2 (b), although 0.5% NC can improve properties, 5% NC into the mass has the highest increase of 132.2% for this type of application of nanocellulose into the mass. There is not a significant increase of the tensile index between 1-layer and 2-layer coatings.
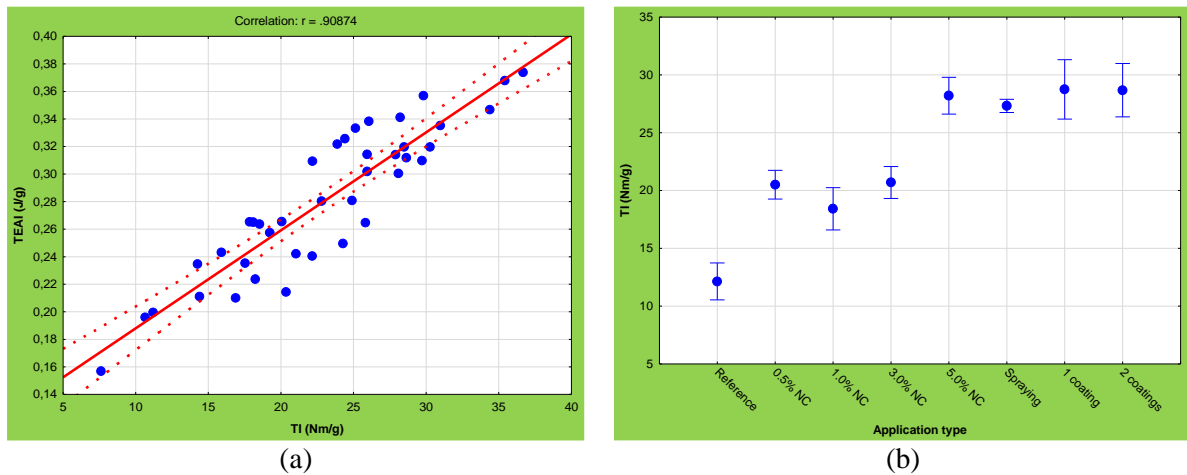
Fig. 2: (a) Dependence of the tensile work absorption on the tensile index, (b) Tensile index results.

In Figure 3, there is a micrograph from the scanning electron microscopy. In the samples with the addition of 5% NC, there are nanofibrils (smaller particles, that are not observed in the reference samples). Nanofibrils are connected with free OH- chemical bonds with cellulose fibrils in the paper. This situation affects positively paper properties when NC is applied. The samples on top are magnified 200× and the samples located on the bottom are magnified 5500×.
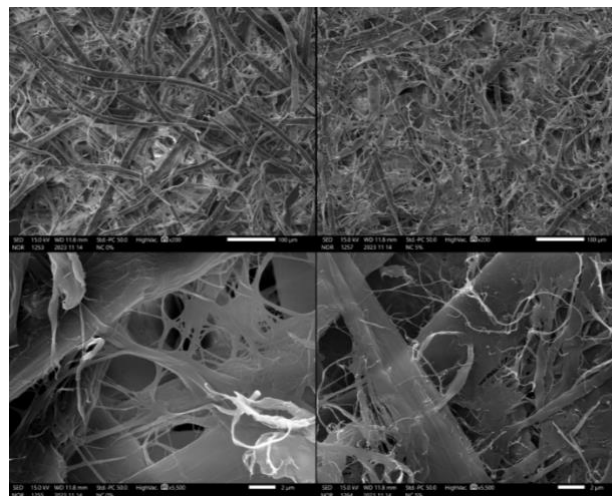
Fig. 3: Scanning electron microscope micrograph.

4.   Conclusion

Spraying NC application seems the most effective with sufficient amount of NC added (3.5% of NC), but also with 1-layer coating with 4.8% of NC application. Usage less than 3% of NC does not affect significantly the properties of samples due to leaking NC into subsieve water in paper production. Positive dependence of the amount NC used during the process of paper production. Colour has not changed significantly with the NC application.

Acknowledgements

References

1. Das, A.K.; Islam, M.N.; Ashaduzzaman, M.; Nazhad, M.M. "Nanocellulose: Its applications, consequences and challenges in papermaking," in *J. Packag. Technol. Res*. 2020, 4, 253–260.
2. Lengowski, E.C.; Júnior, E.A.B.; Kumode, M.M.N.; Carneiro, M.E.; Satyanarayana, K.G. "Nanocellulose in the Paper Making, In Sustainable Polymer Composites and Nanocomposites," in *Springer,* Inamuddin, Thomas, S., Mishra, R.K., Asiri, A.M., Eds.: Cham, Switzerland, 2019; pp. 1027–1066.
3. Li, A.; Xu, D.; Luo, L.; Zhou, Y.; Yan, W.; Leng, X.; Dai, D.; Zhou, Y.; Ahmad, H.; Rao, J.; et al. "Overview of nanocellulose as additives in paper processing and paper products," in *Nanotechnol. Rev*. 2021, 10, 264–281.
4. Michelin, M.; Gomes, D.G.; Romani, A.; Polizeli, M.d.L.T.M.; Teixeira, J.A. "Nanocellulose Production: Exploring the Enzymatic Route and Residues of Pulp and Paper Industry," in *Molecules* 2020, 25, 3411.
5. Latifah, J.; Nurrul-Atika, M.; Sharmiza, A.; Rushdan, I. "Extraction of nanofibrillated cellulose from kelempayan (neolamarckia cadamba) and its use as strength additive in papermaking," in *J. Trop. For. Sci.* 2020, 32, 170–178.
6. Dinesh, G.; Kandasubramanian, B. "Fabrication of transparent paper devices from nanocellulose fiber," in *Mater. Chem. Phys*. 2022, 281, 125707. Si, Y.; Lin, Q.; Zhou, F.; Qing, J.; Luo, H.; Zhang, C.; Zhang, J.; Cha, R. "The interaction between nanocellulose and microorganisms for new degradable packaging: A review," in *Carbohydr. Polym.* 2022, 295, 119899.
7. Spagnuolo, L.; D'Orsi, R.; Operamolla, A. "Nanocellulose for Paper and Textile Coating: The Importance of Surface Chemistry," in *ChemPlusChem* 2022, 87, e002200204.
8. Deng, J.; Zhu, E.-Q.; Xu, G.-F.; Naik, N.; Murugadoss, V.; Ma, M.-G.; Guo, Z.; Shi, Z.-J. "Overview of renewable polysaccharidebased composites for biodegradable food packaging applications," in *Green Chem*. 2022, 2, 480–492.
9. Li, P.; Zhou, M.; Jian, B.; Lei, H.; Liu, R.; Zhou, X.; Li, X.; Wang, Y.; Zhou, B. "Paper material coated with soybean residue nanocellulose waterproof agent and its application in food packaging," in *Ind. Crops Prod.* 2023, 199, 116749.
10. Barbash, V.A.; Yashchenko, O.V.; Gondovska, A.S.; Deykun, I.M. "Preparation and characterization of nanocellulose obtained by TEMPO-mediated oxidation of organosolv pulp from reed stalks," in *Appl. Nanosci.* 2022, 12, 835–848.
11. Lengowski, E.C.; Júnior, E.A.B.; Simon, L.C.; Bolzon de Muniz, G.I.; de Andrade, A.S.; Leite, A.N.; de Miranda Leite, E.L.S. "Nanocellulose Coating on Kraft Paper," in *Coatings* 2023, 13, 1705.
12. TAPPI T 402 sp-08; Standard Conditioning and Testing Atmospheres for Paper, Board, Pulp Handsheets, and Related Products. Technical Association of the Pulp and Paper Industry. Tappi Tappi Press Atlanta: Atlanta, GA, USA, 2013.
13. ČSN EN ISO 1924-2 (500340); Paper and Board—Determination of tensile Properties. Czech Standard Institute: Prague, Czechia, 2009.
14. ČSN EN ISO/CIE 11664-4 (011720); Colorimetry – Part 4: Colorimetric space CIE 1976 L*a*b*. Czech Standard Institute: Prague, Czechia, 2020.

Core-skin morphology analysis of calendered isotactic polypropylene (iPP) foils

M. Mihelčič [1], Miroslav Huskić [2] and Lidija Slemenik Perše [1*]

[1] Faculty of Mechanical Engineering, University of Ljubljana, Aškerčeva Ulica 6, 1000 Ljubljana, Slovenia
[2] Faculty of Polymer Technology, Ozare 19, 2380 Slovenj Gradec, Slovenia

Abstract

Isotactic polypropylene (iPP) foils, incorporating 10 wt% recycled PP, were manufactured through the calendering process on an industrial calendering line. The cooling time-temperature profile was adjusted by altering the hauling speed of the rollers: 2 m/min for iPP1 and 10 m/min for iPP2 foils, respectively. POM microscopy revealed the formation of a characteristic skin-core structure in the iPP2 foils, where iPP1 foils exhibited more layered structure. Nanoindentation measurements further confirmed the observed structures, illustrating that the core layer displayed a higher elastic modulus compared to the skin layer due to an increased degree of crystallinity, confirmed by flash DSC. Additionally, the uneven temperatures of the hauling rollers resulted in anisotropic mechanical properties with higher values of elastic modulus in the inner region of the foil where the hauling roller's temperature was higher.

Keywords: isotactic polypropylene (iPP), foils, calendering, polarized optical microscopy, nanoindentation, flash differential scanning calorimetry, crystallinity.

1. Introduction

Isotactic polypropylene (iPP) is one of the most commonly used polymers in the packaging industry and is becoming increasingly important due to its favourable combination of cost and performance. Moreover, iPP enables a wide range of possibilities for expanding the range of properties through various modifications. Many technologically relevant properties of iPP, such as optical transparency, stiffness, stability, shrinkage, hardness and elasticity, are related not only to its composition but also to its crystalline microstructure, which is closely linked to the processing methods and manufacturing conditions [1].

iPP is often processed with calendering process, mainly in the production of foils in the packaging industry, where the polymer melt is extruded onto rotating rollers that form a foil. It is known that iPP is extremely sensitive to the conditions during its processing and can therefore form different morphologies. The skin-core structure of the foil is formed by rapid cooling of a thin upper part of the skin as opposed to the core, where more relaxed conditions and a longer cooling rate enable the polymer chains to relax and allow the growth of spherulites. The transition region between the thin skin and the core contains an oriented and crystalline structure that differs from the large and isotropic spherulitic structure of the core. The shear flow enhances the crystallization kinetics in the skin and leads to the transition from the spherulitic to the shish-kebab morphology of the polymer [2].

The skin-core microstructure inevitably affects the mechanical and optical properties of polymers, which emphasises the importance of studying skin-core structures with respect to the corresponding degree of crystallinity. Due to the anisotropy of iPP polymer, the focus of the research presented here was to understand how processing parameters affect the formation of skin-core morphology in calendered iPP foils, where processing conditions, i.e., temperatures, on both sides of the foils are not the same. The aim of the present work was therefore to demonstrate the correlation of the structure morphology, mechanical properties and crystallinity on the surface and in the core of calendered iPP foils produced on an industrial calendering machine. The processing factors such as processing temperature, roller speed, roller temperature and the addition of various additives or recycled PP [3] have already been proven to have a significant impact on the processing quality of calendered iPP foils. Therefore, the physical and morphological properties on the macro- and micro-/nanoscale were investigated in the present study.

2. Materials

Commercially available nucleated polypropylene homopolymer (PPH) (Moplen HP640J) intended for extrusion and thermoforming applications of food packaging containers and bottles was purchased from Lyondell Basell.

Isotactic polypropylene foils iPP1 and iPP2 contained 10 wt. % of recycled polypropylene and were obtained from ground self-produced (iPP) foils and thermoformed products.

The iPP foils were produced by Panplast d.o.o. (Logatec, Slovenia) using an industrial single-screw extruder (BG plast, Italy). The production line was equipped with a film die of 700 mm width and three heated calender rollers of 500 mm diameter R_1 (T = 55 °C), R_2 (T = 80 °C) and R_3 (T = 64 °C). The temperature of iPP polymer melt at the extrusion nozzle was 245 °C. The hauling speed for preparing ~0.75 mm thick iPP foils was related to the production capacity, which was 2 m/min for iPP1 and 10 m/min for iPP2, respectively.

3. Methods

The morphology of the cross-section of the extruded foils was analysed using polarized transmitted light using a Leica DM4000M. The specimens were prepared by a thin-layer grinding method, where the iPP foils were encapsulated in a special resin and sanded with sandpaper with grit up to 2400. Afterwards, they were then bonded to cover glass with the same resin, cut and ground again to form a thin layer.

Nanoindentation measurements were performed using an Agilent (USA) G200 XP nanoindenter equipped with a standard three-sided pyramidal Berkovich probe. The elastic modulus and hardness were determined from the measurements performed using the continuous stiffness measurement (CSM) method with a tip oscillation frequency of 45 Hz and a harmonic amplitude of 2 nm. The nanoindentation measurements were performed over the foils' cross-section. Prior to characterization the samples were embedded in epoxy resin and polished. The CSM method was used, where the maximum penetration depth was 4000 nm and the average value from 3000 to 3500 nm depth was used for data analysis in order to mitigate surface effects resulting from sample polishing.

The degree of crystallinity (X_c) of the foil surface on the side that comes into contact with the roller with a higher temperature (R_2, T = 80 °C) (inner surface) and the foil surface on the opposite side (R_1, T = 55 °C) (upper surface) and the central part of the film (core) were determined using Mettler Toledo Flash DSC 1 calorimeter. Samples were cut from a foil under the microscope and placed on the sensor following instructions reported in [4]. The samples were heated/cooled in a temperature range between 15 and 195 °C with a heating/cooling rate of 1000 K/min, except for mass determination where the cooling rate was 30 K/min. The holding time at both temperatures was 0.1 s. The unknown mass of samples measured on flash DSC (m_{FDSC}) was obtained from the measured enthalpies (H) of melting peaks obtained on DSC (H_{DSC}) and flash DSC (H_{FDSC}) according to equation: $m_{FDSC} = H_{FDSC} (m_{FDSC} / H_{DSC})$.

Typical sample weight was 100-150 ng. The degree of crystallinity was calculated by using melting enthalpy of 100% crystallized ($\Delta H_m^0 = 207 \, J/g$). DSC measurements were performed on Mettler Toledo DSC 2 calorimeter with sample mass of 5-10 mg. N_2 flow was 20 mL/min and the heating/cooling rate was 30 °C/min.

4. Results and Discussion

4.1. Morphology studies: POM and nanoindentation measurements of cross-section

POM measurements were carried out to obtain information on the effects of processing conditions (temperature and roller speed) on the morphology (i.e., preferred crystallite shape, orientation and size) of the foils. In the absence of quiescent conditions, polymer crystallizes homogeneously so that there are no differences in the crystalline structure of the surface and the core. It has already been shown [5] and theoretically formulated with the Janeschitz-Kriegl model that under flow conditions precursor materials elongate in the direction of flow, forming structures known as threads or shish forms [6]. After the flow stops, kebabs consisting of lamellae grow radially from shish. The result is a layer known as highly oriented skin.

In general, when observed in polarized transmitted light, the polymer shows bright (45° polarization) or dark (0° polarization) regions depending on the angle between the oriented direction and the polarizer and analyzer. The processing conditions have a strong effect on the thickness of the oriented skin layer, which depends on the temperature of the polymer melt and varies inversely with temperature. It has been shown [7] that at lower level of shear stress, other types of oriented structures are formed as oriented skin, known as sausages and skin lines. These are lines of relatively high orientation with non-oriented regions between them, which in the case of sausages can be significantly wide. The important fact for this study is that grained layers consisting of smaller spherulites can be observed with less flow in the middle part of the foil (core), as also reported by Woodward et al. [8].

Figure 1 and 2 show POM micrographs of iPP1 and iPP2 foils examined in the 45° polarization direction. It can be seen that the alignment of oriented skin and other spherulitic structures was established. In parallel, the same cross-sections of the foils were used for nanoindentation measurements, which provided the distribution of elastic modulus for specific locations on selected cross-sections of the iPP foils.
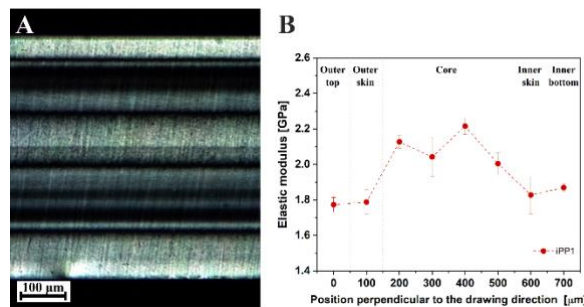
Fig. 1: Cross-section of iPP1 foil: A) POM micrographs and B) nanoindentation elastic modulus.
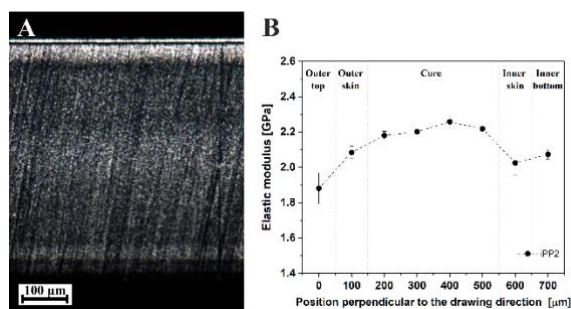
Fig. 2: Cross-section of iPP2 foil: A) POM micrographs and B) nanoindentation elastic modulus.

Both iPP foils show a similar structure with highly oriented skins on both sides followed by darker alternating regions leading to the crystalline core. However, the iPP1 sample exhibited more pronounced layered structure with sharp transitions between different crystalline regions. Importantly, the distribution of the different stratified layers in the outer and inner parts of the foil was not symmetrical, indicating that the crystallization conditions in the outer and inner parts of the foil were not the same. To determine the degree of crystallinity, the DSC and flash DSC measurements were performed.

4.2. DSC and flash DSC measurements

In the first step, DSC results were obtained from the 1st heating at 30 °C/min for iPP1 and iPP2 samples with same composition but differ in the drawing speed (haul-off speed iPP1 < iPP2). The corresponding X_c value of the slower-drawn iPP1 (39.3 %) foil was lower than the X_c value of iPP2 (41.7 %). This result was expected since the drawing process aligns the molecules in the direction of flow and thus facilitates crystallization. At the 2nd heating, both foils showed higher X_c values compared to the 1st heating, and their relative values also reflected the differences in their composition, while the melting peaks obtained at the 2nd heating were monomodal. In addition, the lower X_c values were obtained for iPP1 and higher X_c values for iPP2. The latter can be explained by the longer retention time in the extruder, at a high temperature resulting in polymer decomposition. The results are also consistent with the findings of Fisher and Drummer [9], who found that the crystallinity is lower in foils that were pulled over the rollers slowlier at temperatures similar to ours.

In order to gain further insight into the crystallization behaviour of calendered iPP foils, the main focus was to determine the X_c values of both sides (outer and inner) and the center (core) of the foils using flash DSC measurements. Although the POM measurements were not quantitative in nature, the features visible in the POM micrographs could be correlated to some extent with the X_c values obtained from the flash DSC measurements. It was clear, that the asymmetric stratification of layers could be correlated to the asymmetrical temperature gradients in the production line (causing the outer part to crystallize differently from the inner part of the foil). Nonetheless, the different X_c values of the outer and inner parts of the foil surface ($X_c^{inner} > X_c^{outer}$) confirmed that the inner part of the iPP1 foil was in contact with a warmer roller (80 °C) longer than the outer part, which was exposed to the ambient air temperature.

The massive crystalline layer observed at the inner part of the foil independently supported X_c values obtained from the FSC measurements, i.e., X_c^{inner} (47.4%) $> X_c^{outer}$ (38.1%), while the value of X_c^{core} was 60.1%. The layers were stratified and represented the most prominent feature of the iPP1 foil, in contrast to the observed skin-core morphology of the iPP2 foil. The degree of orientation gradually decreases with increasing distance from the surface, but the core could exhibit a certain degree of orientation, as was confirmed for both iPP samples studied. For iPP2 foil X_c values ((X_c^{outer} (43.1%), X_c^{core} (64.1%) and X_c^{inner} (40.6%)), indicated that crystallinity of the core was higher than that of the skin, which was not distinctly observed from micrographs.

5.   Conclusion

In conclusion, examination of POM images and comparison of iPP foils cross-sections in polarized light showed that a characteristic shear layer appears under the oriented top layer, followed by a core with well-defined crystallinity. In addition, the drawing speed of the foil was high enough to cause a change in temperature and cooling rate (alternating contact with the roller and air), so that the darker regions are also clearly visible. In addition, the distribution of the different layers in the outer and inner parts of the foil was not symmetrical, indicating that the crystallization conditions in the outer and inner parts of the foil were not the same, which is consistent with the elastic modulus values obtained by nanoindentation measurements. The nanoindentation results suggested that the higher values of elastic modulus resulted in higher values of X_c, with the core exhibited higher values of elastic modulus and X_c compared to the oriented skin in both iPP foils.

Acknowledgements

References

1. J. W. Housmans et al., "Structure-property relations in molded, nucleated isotactic polypropylene," *Polymer.*, vol. 50, no. 10, pp. 2304–231, 2009.
2. G. Kumaraswamy, et al., "Shear-enhanced crystallization in isotactic polypropylene. 3. Evidence for a kinetic pathway to nucleation," *Macromolecules*, vol. 35, no. 5, pp. 1762–1769, 2002.
3. M. Mihelčič, et al., "Influence of additives on structural and morphological characterisation of calendered isotactic polypropylene foils", in *Akademija strojništva 2023, Ljubljana, Slovenia*, 2023, vol. 12, no. 3/6, pp. 74-75.
4. S. Adamovsky and C. Schick, "Ultra-fast isothermal calorimetry using thin film sensors," *Thermochim. Acta*, vol. 415, no. 1-2, pp. 1–7, 2004.
5. H. Janeschitz-Kriegl, "Crystallization modalities in polymer melt processing: Fundamental aspects of structure formation," Wien: Springer-Verlag, 2010.
6. S. Liedauer et al., "On the Kinetics of Shear Induced Crystallization in Polypropylene," *Int. Polym. Process.*, vol. 8, no.3, pp. 236–244, 1993.
7. L. Fernandez-Ballester, et al., "Effect of long chains on the threshold stresses for flow-induced crystallization in iPP: Shish kebabs vs sausages," *Macromolecules*, vol. 45, no. 16, pp. 6557–6570, 2012.
8. A. E. Woodward, "Understanding polymer morphology" , Hanser Pub Inc, 1996.
9. C. Fischer and D. Drummer, "Crystallization and Mechanical Properties of Polypropylene under Processing-Relevant Cooling Conditions with respect to Isothermal Holding Time," *Int. J. Polym. Sci.*, vol. 2016, pp. 11, 2016.

Challenges and solutions to assess the real true stress – true strain response of pure and recycled polymers under large strains

P. Hao [1,*], C. Siebers [2], K. Ragaert [2], F. A. Gilabert [1]

[1] Department of Materials, Textiles and Chemical Engineering (MaTCh), Mechanics of Materials and Structures (MMS), Ghent University, Technologiepark Zwijnaarde 46, 9052, Zwijnaarde, Belgium
[2] Circular Plastics, Department of Circular Chemical Engineering, Faculty of Science and Engineering, Maastricht University, 6162 AL Geleen, The Netherlands

Abstract

The objective of this study is to develop robust characterization techniques to facilitate the design of high-quality recycled plastics. We address the complex task of obtaining thermomechanical responses of both pure and blended thermoplastics. Specifically, we investigate high-density polyethylene (HDPE), polypropylene (PP), and a compounded HDPE/PP blend. Tensile tests were conducted using ISO-527/1A dog-bone specimens. A high-speed 3D stereo Digital Image Correlation (DIC) system synchronized with an infrared camera was employed to measure strain and temperature fields. An accurate constitutive response of the polymer was utilized to quantify rate- and temperature-dependence, as well as phenomena such as self-heating and thermal softening, often observed at medium and high loading speeds. This model effectively characterizes the complex yielding kinematic mechanisms in both pure and blended polymers. Through a hybrid experimental-numerical approach, the model accurately captures the true thermomechanical response of these materials, demonstrating its utility in addressing challenges associated with necking effects. This approach successfully tracks the dynamic yielding process in polymers, mapping local strain and temperature fields in detail. Such detailed understanding is essential for employing advanced simulation techniques in the design and application of recycled polymers. The aim is to achieve performance comparable to that of pure materials, thus enhancing the viability of recycled polymers.

Keywords: thermoplastics, recycled plastics, thermomechanical behavior, necking, FEM, self-heating.

1. Introduction

The blending of polyolefins (POs), such as polyethylene (PE) and polypropylene (PP), have been an active area of research, particularly for recycling mixed polyolefin (MPO) waste using flotation sorting techniques. However, understanding the thermomechanical behavior of these recycled blends poses challenges due to limitations in existing characterization methods. 'Necking' effects, originated from geometric nonlinearity in the specimen, contribute to the nuanced characterization of tensile behavior, especially in highly stretchable polymers [1]. Current approaches to determining strains in these materials do not offer a reliable measure suitable for confidently incorporating into modeling and simulation frameworks, which require an accurate constitutive response of the polymer.

Efforts have been made to decouple geometric nonlinearity from intrinsic material response by approximating true stress-strain curves through comparison of different video-based extensometry techniques [2]. It is also reported that self-heating occurs due to the accumulating plastic dissipation energy when loading speed is increased [3-5]. Additionally, it's well-known that polymers are temperature-dependent and experience thermal softening at elevated temperatures [6, 7]. This thermomechanical coupled response must be quantitatively investigated under non-isothermal conditions.

2. Methods

In this study, a combined experimental-numerical approach was employed to determine the true stress-strain response of both pure polymers and a recycled blend. High-density polyethylene (HDPE) (F4520) and polypropylene (PP) (576P) grades for blow molding and injection molding were supplied by SABIC, The Netherlands. A blend containing 10 wt% 576P was compounded. Pure HDPE and PP samples underwent melt processing under the same conditions as the blend.

2.1. Experiments

Tensile tests were conducted following ISO-527 standards. A loading speed range from 1 to 40 mm/min was selected to investigate rate-dependence and self-heating effects. The tests were performed using an Electropuls Instron E10000 linear-torsion apparatus, equipped with a high-speed stereo Digital Image Correlation (DIC) system paired with an infrared camera. This setup enabled detailed thermomechanical analyses by capturing temperature variations alongside mechanical stress and strain, as depicted in Figure 1.
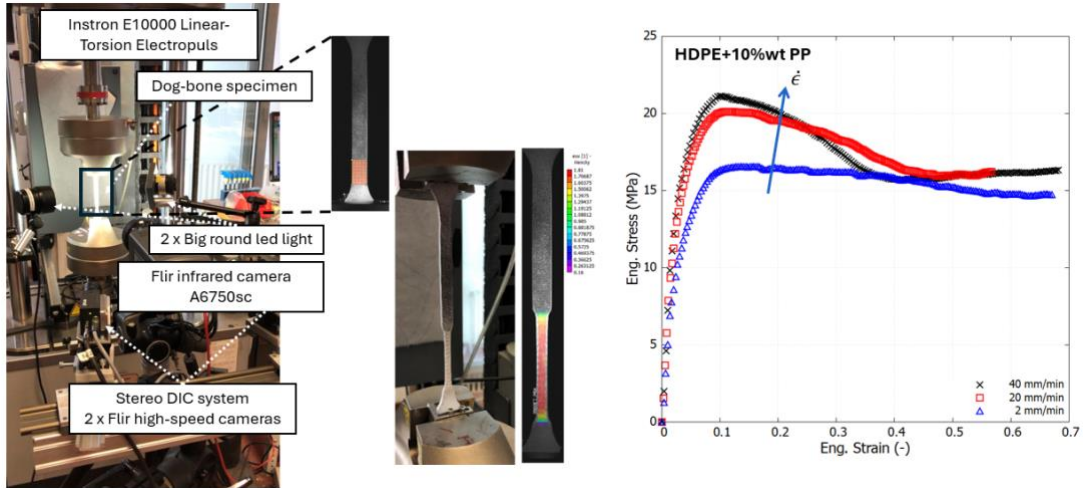
Fig. 1: Instron Electropuls tensile experiment set-up using 3D stereo DIC system combined with IR camera (left) and engineering stress-stress response of the blend at different loading speeds (right).

2.2. Constitutive model

Polymers are widely recognized for their rate and temperature dependence [3-7]. Additionally, various trends in stress-strain curves can be observed from amorphous to semicrystalline polymers, such as the double yield phenomenon. Building on this understanding, a consistent polymer model has recently been developed, tailored for a range of thermosets and thermoplastics [7]. The key evolution of athermal strength allowing the capture of different trends can be described as follows:

$$\dot{s} = H_1(\bar{\varepsilon}) \cdot \left(1 - \frac{s}{s_1}\right) \cdot \dot{\bar{\varepsilon}} + H_2(\bar{\varepsilon}) \cdot \left(1 - \frac{s}{s_2}\right) \cdot \dot{\bar{\varepsilon}} + H_3(\bar{\varepsilon}) \cdot \left(1 - \frac{s}{s_3}\right) \cdot \dot{\bar{\varepsilon}} \tag{1}$$

Full description of these quantities can be found in Ref. [7]. To naturally capture the thermomechanical coupling, the heat balance equation is provided by assuming the dissipation is completely converted to heat:

$$\rho \, c_p \frac{\partial \theta}{\partial t} = \boldsymbol{\sigma} : \boldsymbol{F}^e \boldsymbol{L}^p (\boldsymbol{F}^e)^{-1} + \nabla \cdot \left(k \frac{\partial \theta}{\partial \boldsymbol{x}} \boldsymbol{x}\right) \tag{2}$$

where ρ is the polymer density, c_p constant thermal specific heat and k thermal conductivity. The 2nd-order tensors $\boldsymbol{F}^e$ is the elastic deformation gradients. The plastic velocity gradient expressed in the relaxed configuration is denoted by $\boldsymbol{L}^p$. More details on further considerations adopted for this coupling can be consulted in Ref. [7].

3. Results and discussion

Two types of simulations have been conducted using the advanced polymer constitutive model mentioned above: (i) single element (SE) tests for rapid material evaluation and (ii) full-scale dog-bone simulations for detailed analysis of dynamic yielding mechanisms.
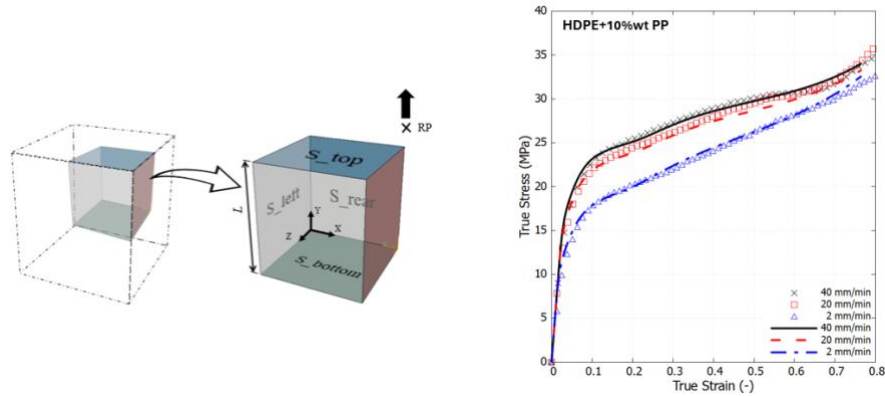
Fig. 2: Single element test and true stress-strain response comparison between experiments and simulations.

To calibrate the model and identify parameters, an in-house Python script incorporating Nelder-Mead optimization and Abaqus was used via SE tests. In this case, the intrinsic material response is a prerequisite. True strain was obtained by averaging the axial strain within the chosen DIC window, while true stress was calculated assuming incompressibility during plastic deformation [2]. Figure 2 shows that the rate dependence is well captured, and the downward trend of curves at high loading speeds is evident in both experimental and simulation results. The drastically increased stress above the strain of 0.7 is attributed to the reorientation of polymer chains, leading to hyperelastic behavior. The obtained material parameters were then applied in the full-scale dog-bone model. Fine calibration was introduced to also capture the effect of geometric non-linearity and material inhomogeneity during the injection process.
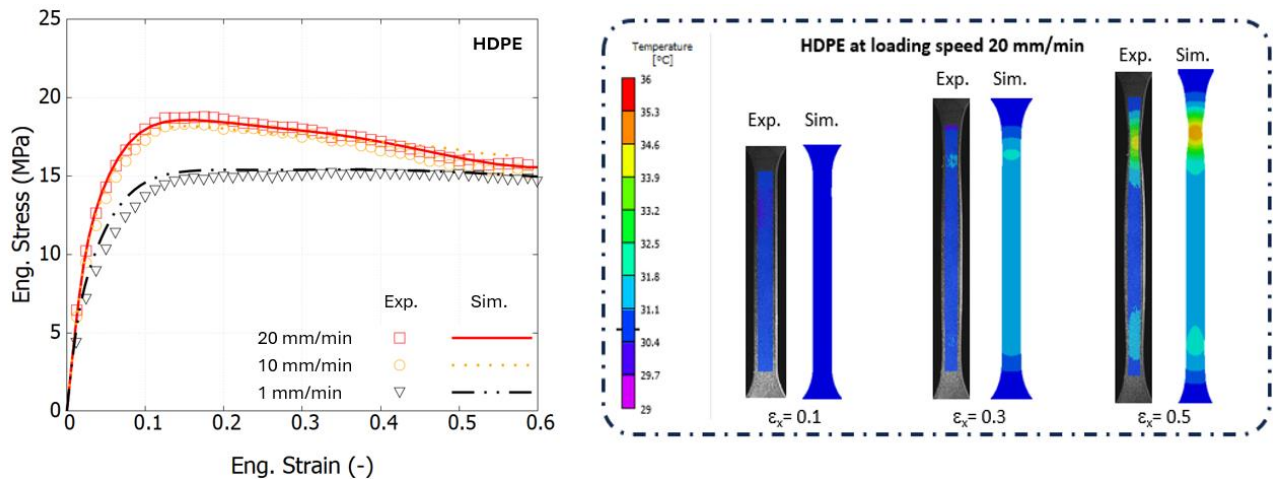
Fig. 3: Comparison of engineering stress-strain curves in dog-bone specimen and local temperature profile of HDPE.

The results of the dog-bone simulation show good agreement with the experimental ones in terms of both global and local responses. The engineering stress-strain curves illustrate different stages during the necking process, including initiation and cold drawing. The local profile reveals that the deformation is not homogeneous throughout the entire dog-bone specimen. At a higher loading speed of 20 mm/min, the temperature increases within the necking region from the initial 30°C to 36°C at a strain of 0.5, while the remaining regions experience lower temperatures, indicating no plastic dissipation. The temperature profile in the simulation clearly demonstrates the dynamic yielding mechanism and suggests the necessity of conducting thermomechanical coupling analyses, supported by evidence from the infrared camera.

4. Conclusion

The proposed approach provides solutions to assess the true stress–true strain response of both pure and recycled polymers under large strains. The recently developed polymer model offers an all-in-one solution to characterize both pure polymers and blends. It can serve as a fast evaluation and high-fidelity simulation for full-scale dog-bone tests. The accurate global response and local profiles show great agreement when compared to the experimental results. The dynamic yielding mechanism that occurs in highly stretchable plastics must be

modeled using rate-dependent material response and thermomechanical coupling analyses. This approach provides a robust evaluation to promote the use of recycled plastics in wider applications.

Acknowledgements

References

1. R. Demets, M. Grodent, K. Van Kets, S. De Meester, and K. Ragaert, "Macromolecular Insights into the Altered Mechanical Deformation Mechanisms of Non-Polyolefin Contaminated Polyolefins," *Polymers*, vol. 14, no. 2, p. 239, 2022.
2. X. Poulain, L. W. Kohlman, W. Binienda, G. D. Roberts, R. K. Goldberg, and A. A. Benzerga, "Determination of the intrinsic behavior of polymers using digital image correlation combined with video-monitored testing", *Int. J. Solids Struct.*, vol. 50, pp. 1869-1878, 2013.
3. E. M. Arruda, M. C. Boyce, and R. Jayachandran, "Effects of strain rate, temperature and thermomechanical coupling on the finite strain deformation of glassy polymers," *Mech. Mater.*, vol. 19, no. 2–3, pp. 193–212, 1995.
4. D. Garcia-Gonzalez, R. Zaera, and A. Arias, "A hyperelastic-thermoviscoplastic constitutive model for semi-crystalline polymers: Application to PEEK under dynamic loading conditions", *Int. J. Plast.*, vol. 88, pp. 27–52, 2017.
5. P. Hao, S. W. F. Spronk, W. Van Paepegem, and F. A. Gilabert, "Hydraulic-based testing and material modelling to investigate uniaxial compression of thermoset and thermoplastic polymers in quasistatic-to-dynamic regime", *Mater. & Des.*, p. 111367, 2022.
6. V. Srivastava, S. A. Chester, N. M. Ames, and L. Anand, "A thermo-mechanically-coupled large-deformation theory for amorphous polymers in a temperature range which spans their glass transition", *Int. J. Plast.*, vol. 26, no. 8, pp. 1138–1182, 2010.
7. P. Hao, Z. Dai, V. Laheri, and F. A. Gilabert, "A unified amorphous–crystalline viscoplastic hardening law for non-isothermal modelling of thermoplastics and thermosets", *Int. J. Plast.*, vol. 159, pp. 103469, 2022.

On The Measurement of the Width of the Distribution of Retardation Times in Polypropylene (II)

José André[1], José Cruz Pinto[2]

[1] UTC - Engineering and Technology, UDI-Research Unit for Inland Development, Guarda Polytechnic Institute, Guarda Portugal, jandre@ipg.pt
[2] CICECO/Department of Chemistry, University of Aveiro, Aveiro Portugal, jj.cruz.pinto@ua.pt

Abstract

In previous literature, empirical models have been applied to describe and predict the viscoelastic behaviour of polymer materials. For example, the empirical power-law model seems to fit well, but only for short-term data. Such formulations are of some utility in data reduction and extrapolation, but do not allow meaningful physical interpretations and lack generality.

The non-linear creep compliance of a polypropylene (PP) was studied at 30, 40 and 50 ºC, for tensile stresses between 2 and 10 MPa. The model developed, which is based on physical mechanisms (at the molecular scale) responsible for the material's behaviour, yields very good agreement with the experimental data and physically meaningful theoretical parameter values.

Keywords: polypropylene, PP, retardation times, creep, minimum retardation time.

1. Introduction

The stress- and temperature- dependent non-linear creep behavior of polymers was quantitatively modelled as a superposition of a range of activated motions at the molecular scale, covering well-defined space and time-scales.

When we look at the dynamic behaviour of polymers, we recognize the presence of a very large variety of possible and specifiable processes (responses), spanning an extremely wide range of frequencies and cluster sizes within the structure, at any given temperature. That range significantly widens and shifts to lower and lower frequencies (and larger and larger cluster sizes) as the temperature is lowered.

2. Experimental

2.1. Material

This report focuses on semi-crystalline polymer – polypropylene, PP - as 150 mm x 10 mm x 4 mm test specimens, cut and adequately machined from sheets.

2.2. Creep Tests

The creep measurements were carried out with a Zwick Z100 Universal Tensile Testing Machine, equipped with a 2.5 kN load cell and using a Macro extensometer with a deformation measurement range of 100 mm. The strain/force *vs*. time experimental data were automatically collected, stored and treated on a personal computer.

The test specimens were previously conditioned at 23 ºC, and the creep tests were conducted at each selected temperature (30, 40 and 50 ºC) in a thermostatic chamber, under applied stresses of 2, 4, 6, 8 and 10 MPa.

3. Creep Theoretical Model

The main characteristic of a polymer creep process (far from rupture) is a progressive strain increase at a decreasing rate, until this rate reaches either a constant (under viscous flow) or a zero value (for cross-linked amorphous or semi-crystalline polymers).

References 1-3 developed the detailed dynamics of gauche-trans conformational transitions, for the particular case of polymers, as the simplest possible example of localized motions at the molecular scale within the material (assuming entirely free non-entangled chains), but a wide range of other possible motions, both of localized or

cooperative nature, may be shown to yield qualitatively similar physical response behaviour in real bulk materials.

In polymers, single-segment gauche/trans transitions are not possible without the simultaneous participation of a small set of neighboring segments, but the gauche/trans transitions could be taken as a simple and good paradigm for the microscopic modelling of macromolecular materials' responses to a wide range of physical excitations, of which creep is the example studied here.

Given the wide variety of contributing structural elements that are involved in the entire range of cooperative motions, the logical step to take is to consider an adequate distribution of cluster sizes and corresponding retardation times. A long time ago, Feltham [4] had already shown that a log-normal distribution would be a physically reasonable approximation to the retardation spectra of a wide range of viscoelastic materials. As a matter of fact, however, the analysis of the present and other experimental data [3], showed that there is a minimum retardation time, corresponding to the smallest contributing clusters ($n = 1$) in the least constrained local environment within the structure. So, the overall (real) creep compliance may be formulated [1, 3, 5] as

$$D(t) = D_0 + (D_\infty - D_0) \frac{erf\left[b\ln\left(\frac{\tau^*}{\tau_1}\right)\right] + erf\left[b\ln\left(\frac{t}{\tau^*}\right)\right]}{erf\left[b\ln\left(\frac{\tau^*}{\tau_1}\right)\right] + 1}$$

(1)

Feltham [4] has suggested and justified a log-normal relaxation, $H(\theta)$, and retardation time, $L(\tau)$, spectra to interpret the elementary (conformational transition) processes responsible for stress relaxation and creep. Thus, we may write, for the retardation spectrum,

$$L(\tau) = (D_\infty - D_{o,e}) \frac{b}{\sqrt{\pi}} e^{\left[-b^2\left(\ln\frac{\tau}{\tau^*}\right)^2\right]},$$

(2)

The parameter b in Eqs. (1) and (2) turns out to be

$$b = b_0 / \ln(\tau^*/\tau_1),$$

(3)

The effects of temperature and applied stress on the optimised values of b, τ_1, τ^*, D_0 and D_∞ (actual values and physical significance) that best fit the experimental creep strain values are discussed. Figure 1 shows the results of fitting previous equation to the experimental creep compliance curves obtained for PP at 40 ºC.
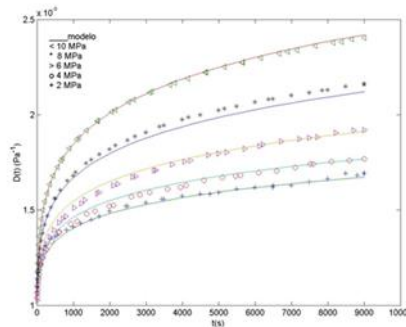
Fig. 1. Model Fitting of the Creep Compliance of PP at 40 ºC.

4. Presentation and physical discussion of model parameter values

The optimised b values are those shown in Table 1 for the whole range of stress values. Table 1 also gives the corresponding predictions for the instantaneous and long-time creep compliances, D_0 and D_∞.

Table 1. Optimised non-linear creep parameter values (b, D_0 and D_∞).

	b at					D_0 (Pa^{-1})	D_∞ (Pa^{-1})
	2 MPa	4 MPa	6 MPa	8 MPa	10 MPa		
30ºC (0,43%)	0.0417	0.0458	0.0518	0.0578	0.0643	$6.20*10^{-10}$	$6.49*10^{-8}$
40ºC (0,67%)	0.0485	0.0532	0.0618	0.0646	0.0688	$7.07*10^{-10}$	$1.95*10^{-8}$
50ºC (0,25%)	0.0507	0.0606	0.0640	0.0669	0.0721	$8.85*10^{-10}$	$1.37*10^{-8}$

The increase of stress and/or temperature yield increases of b, i.e., a decrease in the width of the material's retardation time spectrum, in agreement with previous knowledge [6, 7]. An increase in temperature shortens all individual retardation times, with most significant effects on the longest ones (precisely those that most critically determine the long-term creep behaviour, particularly at low stress), due to their highest activation energies. According to Brostow *et al*. [8, 9] the relaxing capability of the chain segments increases with free volume (within the amorphous phase), temperature and stress, as also found in these experimental and theoretical results.

Both D_0 and D_∞ are the same for all stress values (and all test specimens). Literature agrees [7, 10] on the typical instantaneous and long-time compliance values for semicrystalline polymers. It is worth noting the ability of the model (and calculation algorithm) to predict the correct orders of magnitude from creep data collected for times not shorter than a few seconds and not longer than 9000 s.

The values obtained for the minimum and average retardation times, τ_1 and τ^*, are shown in Tabs. 2 and 3, respectively, for three temperatures and five stress values.

Table 2. Values of the minimum retardation time, τ_1 in s, as a function of temperature and stress, for PP.

	2 MPa	4 MPa	6 MPa	8 MPa	10 MPa
30ºC (0,43%)	$1.13*10^{-8}$	$7.29*10^{-8}$	$7.68*10^{-7}$	$2.52*10^{-6}$	$5.85*10^{-6}$
40ºC (0,67%)	$1.13*10^{-11}$	$1.45*10^{-10}$	$5.68*10^{-9}$	$6.16*10^{-9}$	$1.42*10^{-8}$
50ºC (0,25%)	$2.05*10^{-13}$	$4.98*10^{-11}$	$9.64*10^{-11}$	$1.13*10^{-10}$	$2.46*10^{-10}$

Table 3. Values of the average retardation time, τ^* in s, as a function of temperature and stress, for PP.

	2 MPa	4 MPa	6 MPa	8 MPa	10 MPa
30ºC (0,43%)	$8.89*10^{21}$	$1.27*10^{20}$	$9.05*10^{17}$	$9.70*10^{15}$	$1.51*10^{14}$
40ºC (0,67%)	$1.76*10^{14}$	$1.38*10^{13}$	$3.32*10^{11}$	$5.15*10^{10}$	$8.05*10^{9}$
50ºC (0,25%)	$4.92*10^{11}$	$1.26*10^{10}$	$1.96*10^{9}$	$3.36*10^{8}$	$3.44*10^{7}$

With the optimum predicted values for b, τ_1, τ^*, D_0 and D_∞ (at each temperature and stress), the corresponding retardation time spectra were generated.

Figure 2 shows that increases in the applied stress and temperature decrease the width of the PP spectra. As physically expected, the spectra are also shifted to shorter retardation times when any of the above two variables increases.

It is worth noting that the retardation times span a very wide range of values, from less than 1 s to almost 10^{21} s, which illustrates the very significant cooperativity of the behaviour at temperatures well below the polymer's glass transition temperature.
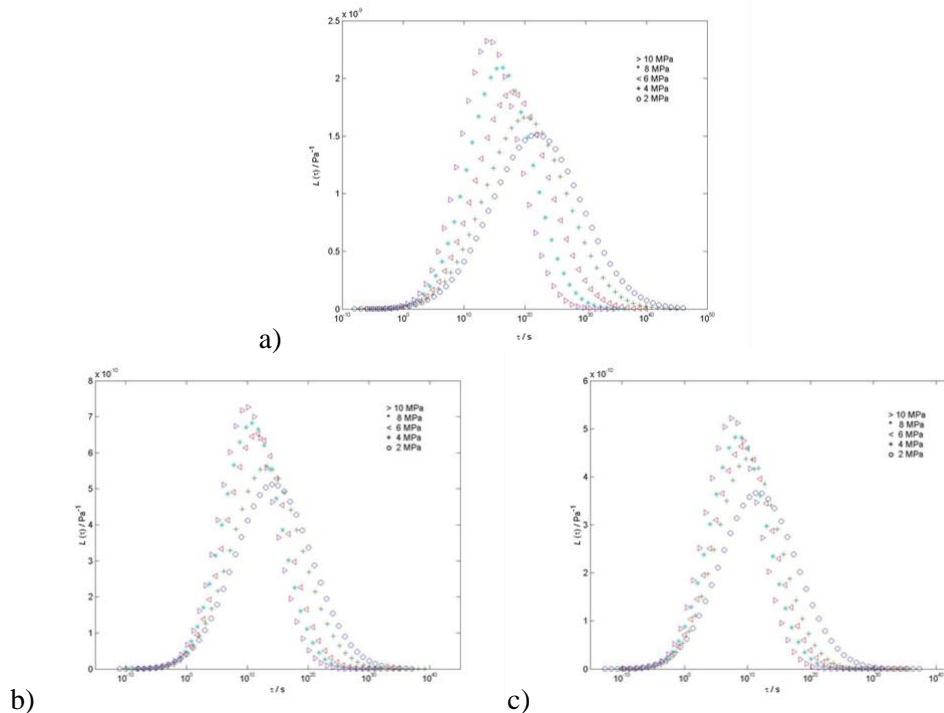
Fig. 2. Retardation time spectra of PP, at 2, 4, 6, 8 and 10 MPa,
and a) 30, b) 40, and c) 50°C.

5. Conclusion

The model successfully predicts the main features of the behavior (Fig. 1), namely its non-linearity, degenerating into full linearity at very low stresses. The correct order of magnitude has been predicted for the infinite time compliance, D_∞, despite the limited time-scale of the experiments ($< 10^4$ s).

The model yields very good agreement with the experimental data, as well as meaningful parameter values in terms of the physical mechanisms (at the molecular scale) responsible for the behaviour of a wide range of viscoelastic polymer materials.

References

1. J.R.S André, "Fluência de Polímeros – Fenomenologia e Modelação Dinâmica Molecular", Ph D dissertation; Departamento de Engenharia Cerâmica e do Vidro, University of Aveiro, 2004.
2. J. R. S. André, J. J. C. Cruz Pinto, "Time-temperature and Time-stress Correspondence in Non-linear Creep. Experimental Behaviour of Amorphous Polymers and Quantitative Modelling Approaches", *e-polymers*, nº. 79, pp. 1-18, 2004.
3.] J.J.C Cruz Pinto; J.R.S. André, "Creep Behaviour of Viscoelastic Polymer Materials", *Advanced Materials Forum II*, pp.759-762, 2004.
4. P. Feltham: *British Journal of Applied Physics*, vol. 6, pp. 26, 1955.
5. J.J.C Cruz Pinto and J.R.S. André, *Analytical Molecular Dynamics of Amorphous Condensed Matter: Thermal and Non-Linear Response Behaviour*, Springer Nature, In press.
6. L.E. Nielsen, *Mechanical Properties of Polymers and Composites*, Dekker, New York, 1974.
7. J. D. Ferry, *Viscoelastic Properties of Polymers*, 3rd Edition, John Wiley & Sons, New York, 1980.
8. Brostow, W., D'Souza, N. A., Kubát, J., Maksimov, R. D., "Service Performance of Polymeric Materials: Prediction from Short-term Tests", *International Journal of Polymeric Materials*, vol. 43, nº 3-4, pp. 233-248, 1999.
9. A. E. Akinay, W. Brostow, "Long-Term Performance of Polymeric Materials from Short-Term Tests: Prediction of the Stress Shift Factor from a Minimum of Data", *Polymer,* vol. 42, pp 4527-4532, 2001.
10. E. Riande, R. Díaz-Calleja, M. G. Prolongo, R. M. Maseoja, C. Salom, *Polymer Viscoelasticity – Stress and Strain in Practice*, Marcel Dekker, Inc., New York, 2000.

Synthesis of Polymer Nanocomposites Reinforced with Graphene Oxide

Sopio mikaberidze[1], Mamuka Maisuradze[1], Natia Jalagonia[2]
[1]Georgian Technical University
[2]Ilia Vekua Sukhumi Institute of Physics and Technology

Abstract:

Since the beginning of the new millennium, the concept of "3D" has firmly entered our daily life. 3D printing technologies open up new possibilities in creativity, science, technology and everyday life. A 3D printer, or three-dimensional printing machine, is a unique modern tool with which we can print both small and large objects. In 3D printing technology, a digital model of the structure of the object is initially created in the computer, which interacts with the printer and starts forming the product layer by layer as a result of the corresponding command. The advantages of 3D printing compared to conventional printing are high speed, simplicity and relatively low cost. That is why this work deals with the synthesis of polymer nanocomposites reinforced with graphene oxide, where polydimethylsiloxane is used as a matrix. First, graphene oxide was synthesized by the modified Hammers' method and mixed with polydimethylsiloxane at different percentage concentrations. Polydimethylsiloxane was dissolved in chloroform and mixed by ultrasonication for homogenous dispersion of graphene oxide plates. We removed solvent from the resulting mixture and made 1 mm thick polymer filaments using an extruder. Here is important to select the temperature regime and relevant solvent for the production of polymer nanocomposites in order to obtain final products with desired properties

Keywords: Graphene oxide, Polydimethylsiloxane, Extruder, Filament

1. Introduction

21th century is often called the century of polymers, because if we look around, we are surrounded by polymers everywhere: at home, in transport, and at work. We can meet polymers, more precisely polymer materials, in many products [1].

First of all, polymer composite materials are distinguished by their mechanical properties and resistance to heat, much higher than pure polymers. Another advantage of composites is that they can take any shape. The formation of products is relatively cheap and of high quality, which requires less work. Also, polymer composite materials are characterized by durability, thermal stability, and have a relatively low price compared to metal alloys [2-3].

One of the methods of preparing polymer composites is melt mixing. The melt mixing method of preparing polymeric materials involves melting the polymer followed by the addition of nanomaterials piece by piece. The melt compounding process is influenced by the following factors, the type of polymer and nanoparticles, temperature, and the process duration. Well melt mixing of polymeric materials can be done with shearing or extruders. This process allows a continuous, fast and easy transformation of raw materials into desired products. However, high temperatures during the melt compounding process can cause thermal degradation of the polymer. Therefore, it is important to select the temperature regime for the production of polymer nanocomposites in order to obtain final products with desired properties.

Graphene-reinforced 3D printing polymer filaments have the potential to advance the manufacturing process of strong, conductive composites. There are many uses for these carbon nanostructured additives in 3D printer filaments, including sensors, electromagnetic and radio frequency shielding devices [4-5].

Fig 1. Extruder for the production of polymer threads

Carbon nanostructures combine with other chemical elements and increase the potential of their use in various fields. Carbon nanostructures are used in adsorbents, energy accumulation and storage systems (batteries, hydrogen storage systems and supercapacitors), catalysts or supports for catalysts, sensors or substrates for sensors, additives in polymers, ceramics, metals and metal alloys, etc. Currently, carbon nanoparticles as nano-fillers are widely found in commercial products of modern technologies [6-7]. Graphene oxide is typically produced by chemical exfoliation of graphite. A well-known technique for obtaining it is the improved Hammers method [8].

A common structural model of graphene oxide shows that its sheet edges are mainly composed of ionizable carboxylic acid groups that are hydrophilic. Meanwhile, the basal plane consists of both hydrophilic oxygen-containing functional groups and hydrophobic aromatic domains.

2.   Results and discussion

Graphene is the world's thinnest material, which is a two-dimensional lattice consisting of hexagons with carbon atoms on the tips. Since its discovery, many studies have been focused on new ways of obtaining this material, its physical and chemical properties, and the creation of new graphene-based nanomaterials. Based on the planned tasks, first, the synthesis and research of graphene oxide was carried out.

a   b
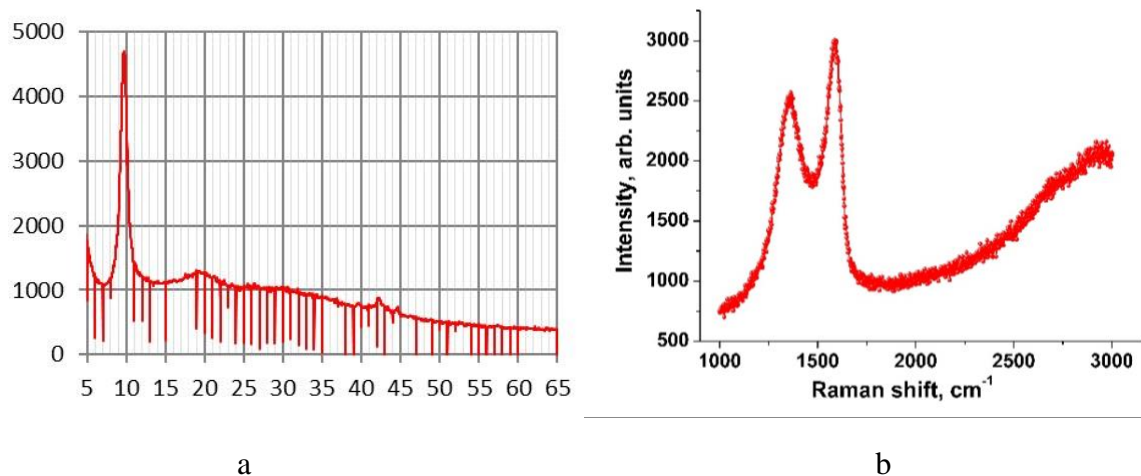
Fig. 2. XRD and Raman spectra of graphene oxide

The modified Hammers method (tested in the literature) was used as a synthesis method and graphene oxide with a layer thickness of >30 was obtained. The obtained graphene oxide was studied by XRD (Figure 2a) and Raman spectral (Figure 2b) methods. XRD structural analysis is a technique used to characterize crystalline materials. With this method, it is possible to determine the orientation or size of a crystal or grain. In XRD (Figure 2a) we observed a peak at 200 which belongs to GO. The Raman spectroscopy results in Figure 2b show a "D" peak at 1590 cm-1 and a "G" peak at 1350 cm-1, which confirmed the lattice deformation.

In the next step, graphene oxide was added to polydimethylsiloxane in different concentrations. In order to homogenous disperse the graphene oxide plates in the matrix, we first dissolved the PDMS in

chloroform, added the graphene oxide plates and stirred for 1 h. Then we removed the solvent from the mixture and obtained polymer nanocomposite plates, which we crushed and made into 1 mm-thick threads using an extruder (Figure 4).
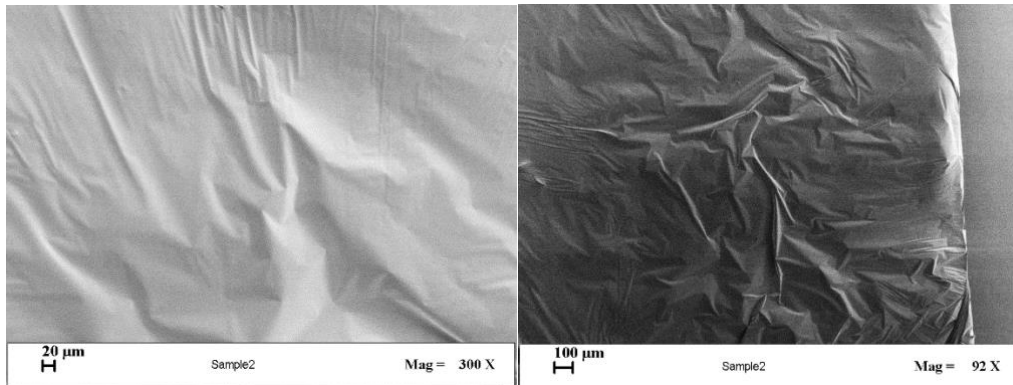
Fig. 3. Micrograph of polymer nanocomposite

The morphology of the polymer nanocomposite was studied by electron microscope (Figure 3), where it can be seen that the graphene oxide plates are fairly evenly distributed in the polymer and no agglomerates are observed.

Fig. 4. Filaments of graphene/polymer composites made by extruder

Conclusion

The synthesis of polymer nanocomposites reinforced with graphene oxide was carried out, where polydimethylsiloxane is used as a matrix. First, graphene oxide was synthesized by the modified Hammers' method and mixed with polydimethylsiloxane at different concentrations. Polydimethylsiloxane was dissolved in chloroform and mixed by ultrasonication for homogenous dispersion of graphene oxide plates. We removed solvent from the resulting mixture and made 1 mm thick polymer filaments using an extruder for further research.

Acknowledgments

References

1. Sun X., Huang C., Wang L., Liang L., Cheng Y., Fei W., Li Y. Recent Progress in Graphene/Polymer Nanocomposites. Adv. Mater. 2021;33:2001105. doi: 10.1002/adma.202001105.
2. Chow W.S., Ishak Z.A.M. Smart polymer nanocomposites: A review. Express Polym. Lett. 2020; 14:416–435. doi: 10.3144/expresspolymlett.2020.35.
3. Luo H., Zhou X., Ellingford C., Zhang Y., Chen S., Zhou K., Zhang D., Bowen C.R., Wan C. Interface design for high energy density polymer21 nanocomposites. Chem. Soc. Rev. 2019;48:4424–4465. doi: 10.1039/C9CS00043
4. G.J. W. Stansbury, M. J. Idacavage. New 3D printable polymeric materials for fused filament fabrication (FFF)Dent. Mater. 32, 54, (2016);
5. E. MacDonald, R. Wicker, Science. Multiprocess 3D printing for increasing component functionality, 353, aaf2093, (2016);
6. Kotsilkov S., Ivanov E. & Vitanov N.K. (2018): Release of Graphene and Carbon Nanotubes from Biodegradable Poly(Lactic Acid) Films during Degradation and Combustion: Risk Associated with the End-of-Life of Nanocomposites Food Packaging Materials. Materials 11, 2346.
7. Tiwari, S.K.; Thakur, A.K.; Adhikari, A.D.; Zhu, Y.; Wang, N. (2020) Current Research of Graphene-Based Nanocomposites and Their Application for Supercapacitors. J. Nanomaterials, 10 (10):2046-2094. doi.org/10.3390/nano10102046.
8. Xu B., Wang H., Zhu Q., Sun N., Anasori B., Hu L., Wang F., Guan Y., Gogotsi Y. (2018) Reduced graphene oxide as a multi-functional conductive binder for supercapacitor electrodes. J. Energy Storage Mater. 12:128–136.

Development of Models to Predict the Properties of Materials Produced of Polymeric Yarns

T. Rolich[1], I. Salopek Čubrić[2], G. Čubrić[3*]

[1] Department of Fundamental Natural and Engineering Sciences, University of Zagreb Faculty of Textile Technology, Zagreb, Croatia

[2] Department of Textile Design and Management, University of Zagreb Faculty of Textile Technology, Zagreb, Croatia

[3] Department of Clothing Technology, University of Zagreb Faculty of Textile Technology, Zagreb, Croatia

Abstract

The constant developments and improvements in the field of material science are in line with the demands of modern society that bring up the quality of the product, its comfort and sustainability in the first plan. Scientists reported a high demand for increased properties of polymeric materials, particularly those that provide an effective barrier to the fluid flow, transfer of heat, air, vapour, gases, and radiation of various origins. Also, the issue of polymer sustainability is highly raised and efforts towards better solutions are given. Still, there is a lack of developed models that may be used to predict the properties of polymeric materials, both aged and non-aged. For the investigation presented in this paper, is used a set of polymeric materials that consist of polyester and polyamide yarns. A total of 12 important properties of these polymeric materials were tested. The testing results were used to develop models that will be able to predict 4 output variables based on 8 input variables of polymeric materials. A linear model upgraded with square members of input variables is shown as the best model, especially for the prediction of heat resistance and water vapour permeability.

Keywords: polymer, yarn, material, model, property, polyester, polyamide

1. Introduction

The constant developments and improvements in the field of material science are in line with the demands of modern society that bring up the quality of the product, its comfort and sustainability in the first plan. Scientists report a high demand for increased properties of textile materials [1-5], particularly those that provide an effective barrier to the fluid flow, transfer of heat, air, vapour, and radiation of various origins. When the advanced functional materials used to produce sportswear are observed, every segment related to the material comfort is the one that needs to be observed and improved. In this type of product, structure regularity and accurate identification have a significant impact on product quality. Studies on the analysis of material structure (specifically, fabrics) have revealed that most issues encountered during analysis are related to the anisotropic properties of such materials. Consequently, despite the large number of published studies, more effort should be directed toward the development of new methods applicable to a specific type of material, as well as the comparison of different methods in order to define a more reliable method for the specifics of the materials observed.

The investigation presented in this paper is therefore forwarded to the development of models that will be able to predict the properties of polymeric materials. To get data related to the properties of polymeric materials, 12 different properties of polymeric were tested.

2. Methodology

2.1. Materials

For the experiment referring to the development of models for polymeric materials, a set of 40 polymeric materials was produced. For the production polyester and polyamide yarns were used. The materials were produced as knitted fabrics consisting of 100% polyester yarn (PES), 100% polyamide yarn (PA6, PA6.6.), as well as with the addition of elastane yarns along with polyester and polyamide. The overview of yarns used is presented in Table 1.

Table 1 Overview of yarns used

Nr.	Polymer	Yarn fineness
1	100% PA 6	18 tex
2	100% PES	18 tex
3	100% PA6.6 (recycled)	18 tex
4	100% PA6.6	18 tex
5	100% PA6.6	15 tex
6	100% PA6.6	17 tex
7	100% PES	19 tex
8	100% PA6.6	17 tex

2.2. Testing Methods

All produced materials were tested for 11 physical-mechanical properties. So, polymeric materials were tested for thickness (d), force at break in the direction of wales (Fp1), force at break in the direction of courses (Fp2), elongation at break in the direction of wales (εB1), elongation at break in the direction of wales (εB2), bursting force (Fb), porosity (CF), heat resistance (Rct), water vapour permeability (W), overall moisture management capacity (OMMC), and drying time (VS). The thickness of polymeric materials was measured following the principles described in ISO standard [6]. For the measurement is used a thickness gauge meter DM - 2000 produced by Wolf Messtechnik GmbH. During the measurement, the pressure of the device was set to 1 kPa. Force at break and elongation at break were measured using the Statimat M tensile tester produced by Textechno. For testing was applied a strip method as described in the ISO standard [7]. A burst tester produced by Apparecchi Branca was used to measure the bursting force. The diameter of the specimen was 50 $\pm$ 1 mm and measurements were carried out following the ASTM standard [8]. Finally, the parameters describing the moisture management property were tested using the Model M290 moisture management tester produced by SDL Atlas. The measurements were performed following the ATTC standard [9].

2.3. Modelling

The goal of this research was to create a regression model that will be able to predict 4 output (dependent) variables based on 8 input (independent) variables. The overview of variables is presented in Table 1.

Table 2 Setup of variables for the development of models

Input variables	Output variables
➢ thickness - d [mm] ➢ mass per unit area - m [g m^{-2}] ➢ force at break in the direction of wales - Fp1 [cN] ➢ force at break in the direction of courses - Fp2 [cN] ➢ elongation at break in the direction of wales - εB1[%] ➢ elongation at break in the direction of wales - εB2 [%] ➢ bursting force - Fb [N] ➢ porosity - CF [%]	➢ heat resistance - Rct [m^{2}KW^{-1}] ➢ water vapour permeability - W [g/cm^{2}h] ➢ overall moisture management capacity - OMMC [-] ➢ drying time - VS [s]

The two regression models were developed:

$$y_p^{(1)} = c_0 + \sum_{i=1}^{k} a_i x_i \tag{1}$$

$$y_p^{(2)} = c_0 + \sum_{i=1}^{k} a_i x_i + \sum_{i=1}^{k} b_i x_i^2 \tag{2}$$

The first is a linear model and the second is a linear model upgraded with square members of input variables. Linear models were realized, and results were obtained using the MATLAB R2022a software package.

3. Results and Discussion

The original data are presented in Figure 1, while the results of both models in Table 3.

a.

b.

c.

d.
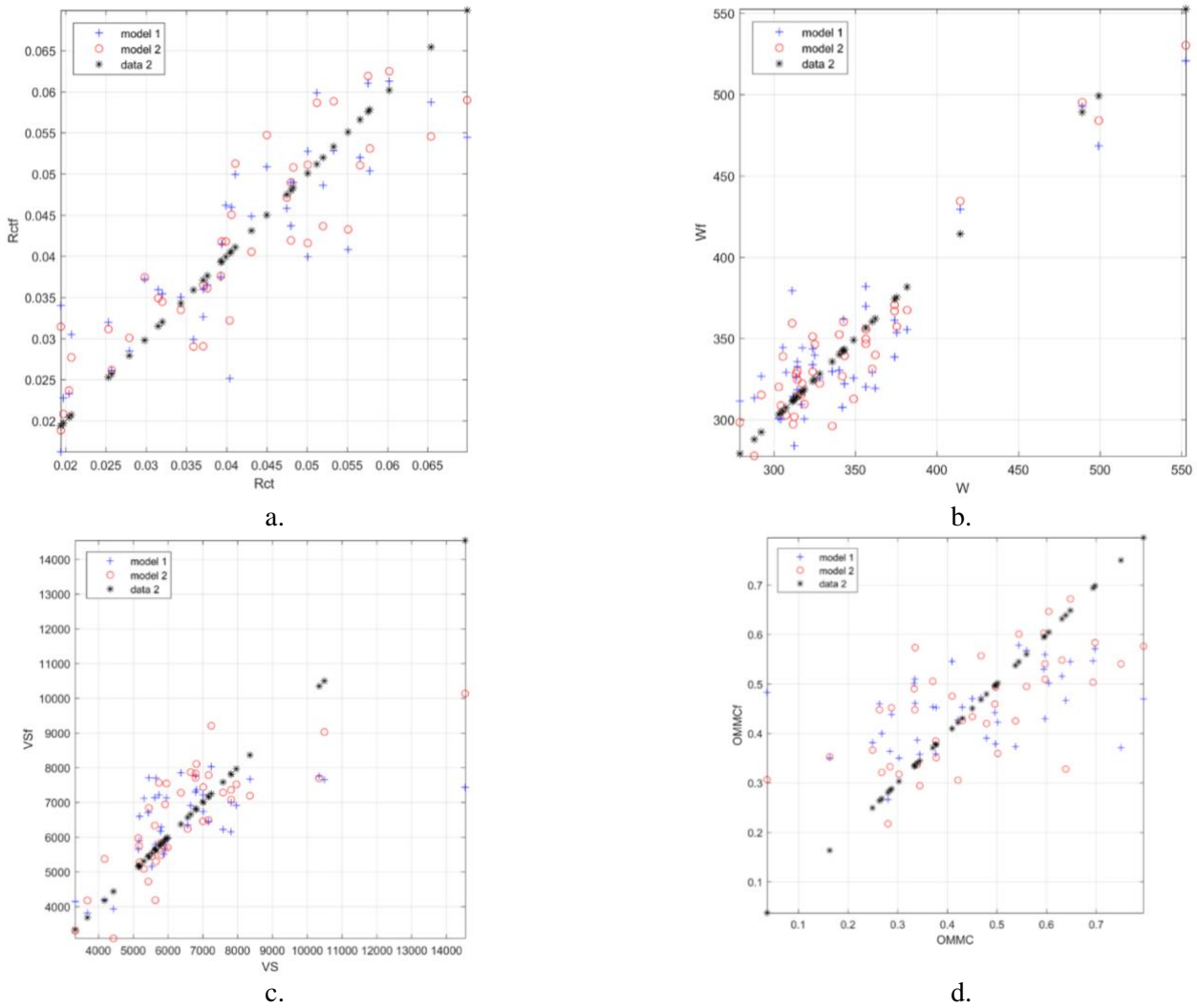
Fig. 1: Original output data obtained from the first and second models for output variable: a. RCT, b. W, C. VS, d. OMMC

Table 3 Results of developed models

	r	MAE	RMSE	R-squared
Rct1	0.8627	0.0051	0.0066	0.7442
Rct2	0.8863	0.0049	0.0061	0.7855
W1	0.8921	21.3594	25.2731	0.7958
W2	0.9431	15.0237	18.5951	0.8895
OMMC1	0.4437	0.1140	0.1493	0.1969
OMMC2	0.6523	0.0987	0.1263	0.4256
VS1	0.5694	1043.4654	1595.6080	0.3242
VS2	0.7798	906.4454	1215.1655	0.6080

Legend: r - coefficient of correlation, MAE - mean average error; RMSE - root-mean-square error; R-squared - coefficient of determination

Table 3 shows that the second regression model is better than the first regression model for all 4 output variables (Rct, W, OMMC and VS), for all model accuracy values (correlation coefficient, MAE, RMSE and R-squared), which was to be expected because the second regression model is an upgrade of the first regression model. For the observed dataset, both regression models had the worst results for the output variable OMMC and the best results for the output variable W and Rct.

4. Conclusion

The aim of the study presented in this paper was to develop models capable of predicting the properties of polymeric materials made from polyester and polyamide yarns. Of the two models developed, a linear model

upgraded with square members of the input variables better describes the output variables for all model accuracy values. The best results of this model are obtained for the properties of heat resistance and water vapour permeability. The results are to be used by practitioners in the field of polymer material design to predict the optimal values of the observed output variables. Future research is to be directed towards developing models with a larger number of polymer materials to obtain a more accurate model for predicting the output variable overall moisture management capacity.

Acknowledgements

References

1. M. Helmi, S. Tashkandi and L.Wang, "Design of sports-abaya and its thermal comfort evaluation," *Text. Res. J.*, vol. 92, pp. 59-69, 2022.
2. J. Fan and H.W.K. Tsang, "Effect of Clothing Thermal Properties on the Thermal Comfort Sensation During Active Sports," *Text. Res. J.*, vol. 78, pp. 111-118, 2008.
3. I. Salopek Čubrić, G. Čubrić, I. Katić Križmančić and M. Kovačević, "Evaluation of Changes in Polymer Material Properties Due to Aging in Different Environments," *Polymers*, vol. 14, pp. 1682, 2022.
4. I. Katić Križmančić, I. Salopek Čubrić, V. M. Potočić Matković and G. Čubrić "Changes in Mechanical Properties of Fabrics Made of Standard and Recycled Polyester Yarns Due to Aging" *Polymers*, vol. 15, pp. 4511, 2023.
5. F.P. La Mantia, R. Scaffaro, M. Baiamonte, M. Ceraulo and Mistretta, M.C. "Comparison of the Recycling Behavior of a Polypropylene Sample Aged in Air and in Marine Water," *Polymers*, vol. 15, pp. 2173, 2023.
6. ISO 5084:1996 Textiles - Determination of thickness of textiles and textile products
7. ISO 13934-1:2013 Textiles - Tensile properties of fabrics - Part 1: Determination of maximum force and elongation at maximum force using the strip method
8. ASTM D3787 Textile Ball Burst Testing. ADMET, Inc.: Norwood, MA, USA, 2020.
9. AATCC TM 195-2021 Liquid Moisture Management Properties of Textile Fabrics